Supplementary Information

Highly efficient and well-controlled ROP and copolymerization of cyclic esters using a cesium complex

Shweta Sagar[a], Himadri Karmakar[a], Priyanku Nath[a], Alok Sarkar[b], Vadapalli Chandrasekhar*[c,d], Tarun K. Panda*[a]*

Table of Contents

Table TS1: Crystallographic data and refinement parameters of complex **2.**

Crystal parameters	**2**
CCDC NO.	2249742
Empirical formula	$C_{45}H_{58}CsN_4P$
Formula weight	818.83
T (K)	293(2)
λ (Å)	0.71073
Crystal system	Monoclinic
Space group	$P2_1$
a (Å)	12.1165(5)
b (Å)	13.9157(8)
c (Å)	13.0991(8)
α (°)	90
β (°)	94.688(5)
γ (°)	90
V (Å^3)	2201.2(2)
Z	2
D_{calc} (g cm^{-3})	1.235
μ (mm^{-1})	0.911
F(000)	852
Theta range for data collection	2.928 to 28.951 deg.
Limiting indices	$-13 \leq h \leq 15$, $-18 \leq k \leq 18$, $-17 \leq l \leq 17$
Reflections collected / unique	18556 / 9119 [R(int) = 0.0349]
Completeness of theta	99.8 %
Absorption correction	Multi-scan
Max. and min. transmission	1.00000 and 0.48227
Refinement method	Full-matrix least-squares on F^2
Data / restraints / parameters	9119 / 1 / 473
Goodness-of-fit on F^2	0.975
Final R indices [I>2Sigma(I)]	R_1 = 0.0342, wR_2 = 0.0658
R indices (all data)	R_1 = 0.0457, wR_2 = 0.0695

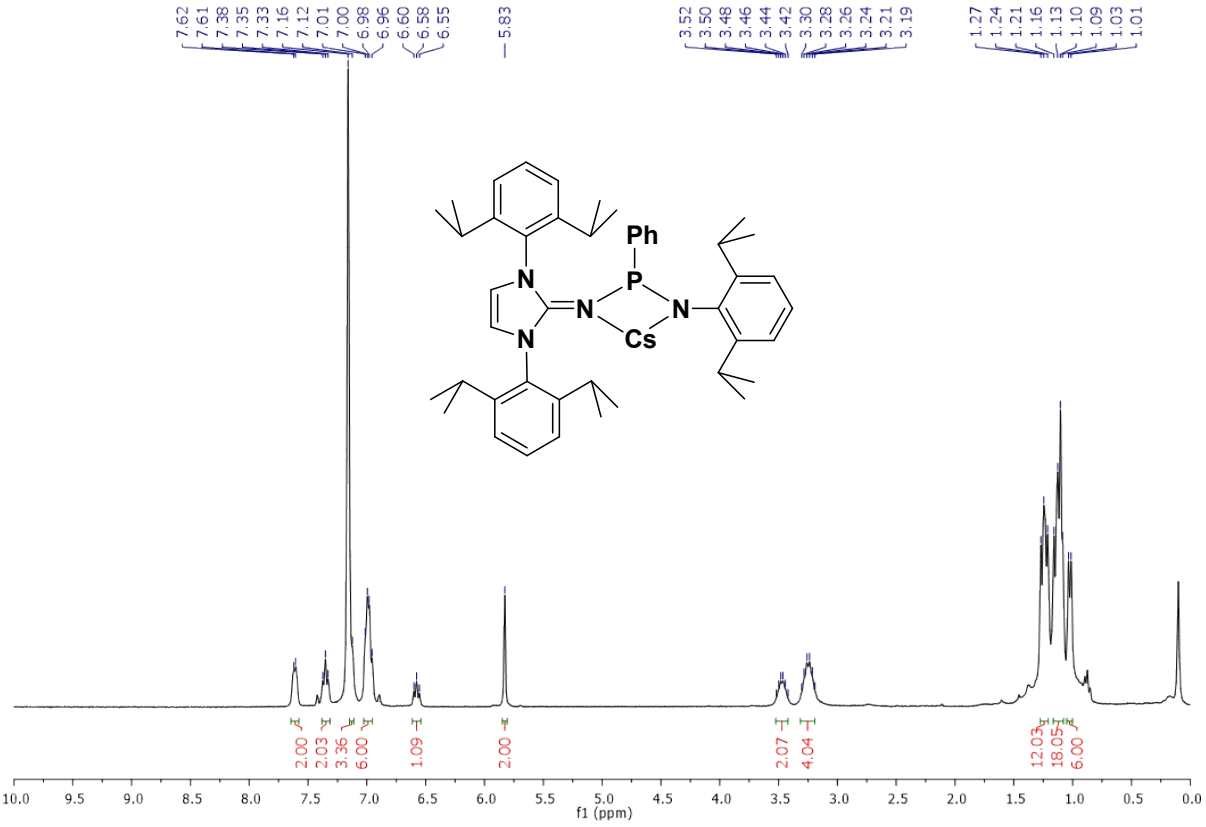

Figure FS1. ^{1}H NMR (400 MHz, C_6D_6, 25 ˚C) of **2.**

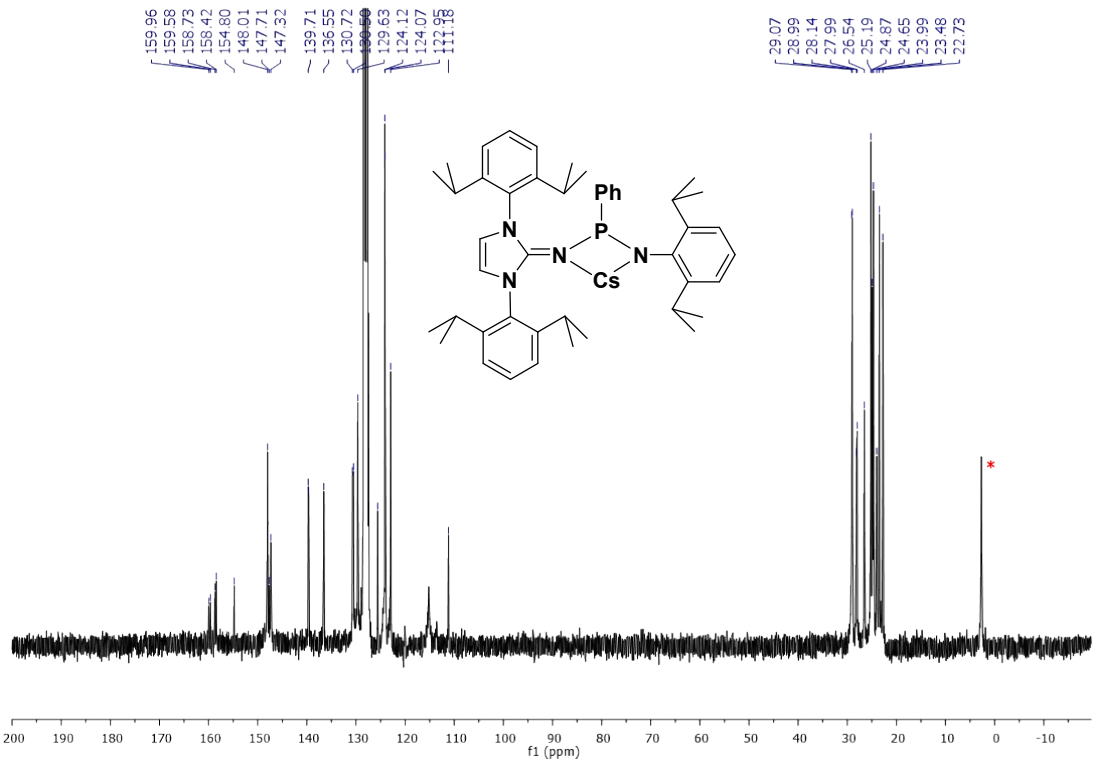

Figure FS2. $^{13}C\{^{1}H\}$ NMR (75 MHz, C_6D_6, 25 ˚C) of **2** (* $HN(SiMe_3)_2$)**.**

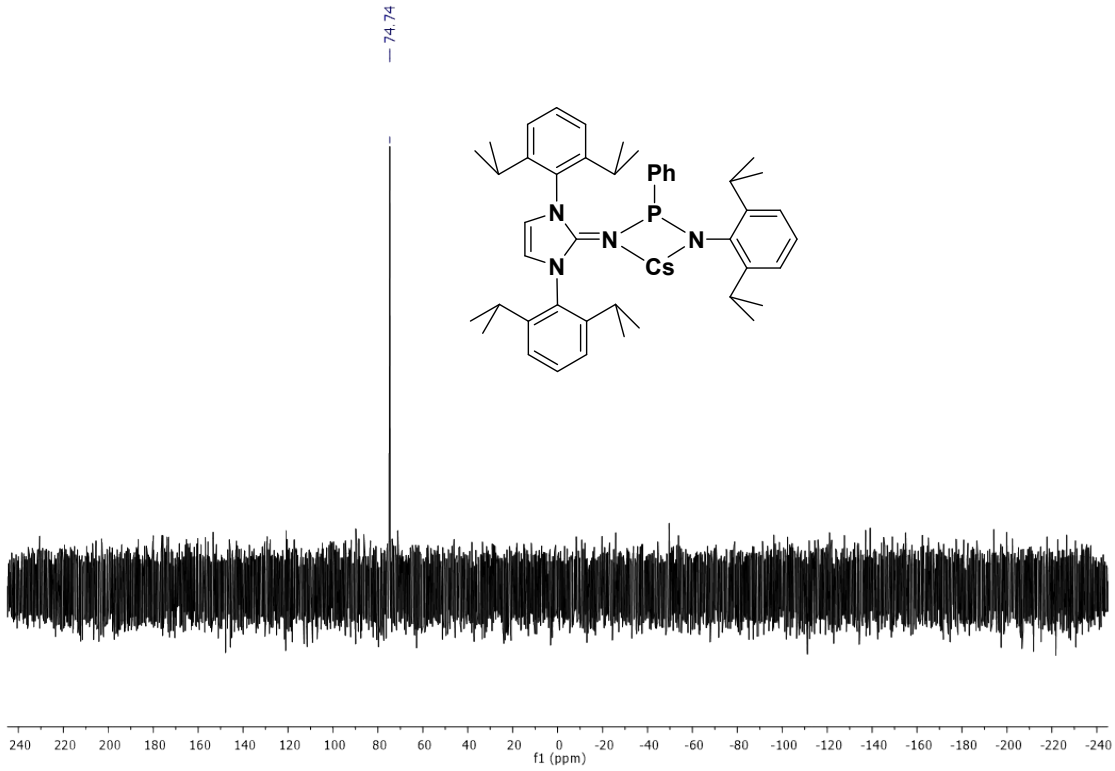

Figure FS3. $^{31}P\{^{1}H\}$ NMR (121.5 MHz, C_6D_6, 25 ˚C) of **2**.

General

All manipulations involving air- and moisture-sensitive organometallic compounds were carried out under argon using the standard Schlenk technique or argon-filled glove box. Polymerization reactions were carried in dried Schlenk tube equipped with magnetic stirrer. In a typical procedure, first the monomer (ε-CL, *rac*-LA) was added to the solution of catalyst (0.013 g, 0.03 mmol) in toluene (1 mL). Then the solution was stirred at required temperature for a desired reaction time after which the solution was quenched by adding one drop of 2 N HCl and methanol. The solution was concentrated in vacuum and polymer was recrystallized from dichloromethane and hexane followed by methanol precipitation. The final polymer obtained was dried under vacuum to constant weight.

Synthesis of ligand [Im^{tBu}NP(Ph)NH(Dipp)] (1-H): The ligand was prepared by the previously published procedure.[5]

Synthesis of [κ^2-{NHI^{Dipp}P(Ph)NDipp}Cs] [Dipp = 2,6- diisopropylphenyl] (2): In an oven-dried 25 ml Schlenk flask, ligand **1-H** (500 mg, 0.728 mmol) was taken and dissolved in 10 ml toluene. Then $CsN(SiMe_3)_2$ (214 mg, 0.728 mmol) was added to it and stirred at 70 °C for 24

h. Next, the solvent was evaporated and the residue was washed with hexane. The crude product was recrystallized from a THF/hexane mixture. Yield: 465 mg, 78%. ^{1}H NMR (300 MHz, C_6D_6, 298 K): δ_H 7.61 (d, *J* = 3 Hz, 2H, Ar-*H*), 7.35 (t, *J* = 7.5 Hz, 2H, Ar-*H*), 7.16 -7.12 (m, 3H, Ar-*H*), 7.01 - 6.96 (m, 6H, Ar-*H*), 6.58 (t, *J* = 7.5 Hz, 1H, Ar-*H*), 5.83 (s, 2H, NC*H*), 3.52 - 3.42 (m, 2H, C*H*(CH_3)$_2$), 3.30 - 3.19 (m, 4H, C*H*(CH_3)$_2$), 1.24 (t, *J* = 9 Hz, 12H, CH(C*H*$_3$)$_2$), 1.16 - 1.09 (m, 18H, CH(C*H*$_3$)$_2$), 1.02 (d, *J* = 6 Hz, 6H, CH(C*H*$_3$)$_2$) ppm. ^{13}C{^{1}H} NMR (75 MHz, C_6D_6, 298 K): δ_C 159.7 (d, NHI-*C*=N), 158.5 (d, Ar*C*-N), 154.8 (Ar*C*-N), 147.7 (t, Ar-*C*), 139.7 (d, Ar-*C*), 136.5 (Ar-*C*), 130.6 (d, Ar-*C*), 129.6 (Ar-*C*), 125.6 (Ar-*C*), 124.1 (d, Ar-*C*), 122.9 (Ar-*C*), 111.2 (NHI-*C*=*C*), 29.1 (d, *C*H(CH_3)$_2$), 28.1 (d, *C*H(CH_3)$_2$), 26.5 (*C*H(CH_3)$_2$), 25.2 (CH(*C*H$_3$)$_2$), 24.8 (CH(*C*H$_3$)$_2$), 24.6 (CH(*C*H$_3$)$_2$), 23.9 (CH(*C*H$_3$)$_2$), 23.5 (CH(*C*H$_3$)$_2$), 22.7 (CH(*C*H$_3$)$_2$) ppm. ^{31}P{^{1}H} NMR (121.5 MHz, C_6D_6, 298 K): δ_P 74.7 ppm. Elemental analysis for $C_{45}H_{58}CsN_4P$ (818.8). Calcd for C 66.01, H 7.14, N 6.84; Found C 65. 87, H 6.98, N 6.59.

Typical polymerization of lactone

First, the monomer (lactone) was added to a solution of the catalyst in toluene. After the solution was reacted at ambient temperature for the desired reaction time, it was quenched with acidified methanol. Then the solution was concentrated in a vacuum and the polymer was recrystallized with dichloromethane and hexane. The final polymer was filtered and dried under vacuum to constant weight.

DSC Analysis

DSC studies were carried out on a SDT Q200 DSC instrument, with a heating rate of 10 ˚C min^{-1} under N_2 flow (50 ml min^{-1}). DSC technical indicators are as follows: maximal sensitivity, 0.2 mw; calorimeter accu*rac*y, prior to 1%; calorimeter precision, prior to 1%; temperature accu*rac*y, < 0.1 ˚C; temperature precision, < 0.01 ˚C. An unsealed Al pan with a 2.0 mg sample was used in the experiments. For ΔH measurements, the DSC system was calibrated with indium (m.p. 156.60 ˚C; ΔH_{fus} = 28.45 J g^{-1}).

TGA analysis

TGA analysis was carried out using a SDT Q600 TGA instrument. TGA technical indicators are as follows: balance sensitivity, 0.1 mg; balance accu*rac*y, prior to 0.1%; balance precision, prior to 0.02%; weighting precision, reach to 10 ppm; temperature precision, ±2 ˚C (measure

sample). TGA experiment was carried out under N_2 dynamic atmospheres at a flow rate of 10 mL min^{-1}. 2 mg PCL/PLA sample was heated from 40 to 500 ˚C at 10 ˚C min^{-1} in a nitrogen atmosphere (50 ml min^{-1}).

Details of the Kinetics Study for *rac*–LA Polymerization

[κ²-{NHI^{Dipp}P(Ph)NDipp}Cs] (2) as catalyst

To explore the reaction kinetics, we perfomed a series of experiments to verify the reaction order. For this, we prepared different concentrations of catalyst **2** (0.01, 0.02, 0.03, 0.04, 0.05 M) in $CDCl_3$ (0.5 mL) and *rac*-LA (0.228 g, 2.0 mmol) was added at room temperature. The solution was observed for ^{1}H-NMR after heating at ambient temperature for required time intervals. The kinetic plots for $[LA]_0/[LA]$ vs cat **2** were found to be linear which indicates that there is first order dependence on *rac*-LA concentration (Figure FS4). Therefore, the rate expression can be summarized as $-d[LA]/dt = k[LA]^1 [\kappa^2\text{-}\{NHI^{Dipp}P(Ph)NDipp\}Cs]^x = k_{obs}[LA]^1$ where $k_{obs} = k_{app}[\kappa^2\text{-}\{NHI^{Dipp}P(Ph)NDipp\}Cs]^x$. Also, a plot of $\ln k_{obs}$ versus $\ln[\kappa^2\text{-}\{NHI^{Dipp}P(Ph)NDipp\}Cs]$ is linear indicating the order of $[\kappa^2\text{-}\{NHI^{Dipp}P(Ph)NDipp\}Cs]$ is x= 1.1 (Figure FS5). Since the polymerization reactions showed first order dependence, it substantiates that there is a presence of only one initiator and comprehensively, it's a second order rate law which can be expressed as

$$\text{rate} = -d[LA]/dt = k_p [cat]^1 [LA]^1$$

The activation parameters for the ROP or *rac*-LA in $CDCl_3$ were found to be $\Delta H^{\ddagger}$= 36.6 kJ/mol K and $\Delta S^{\ddagger}$= -11.2 J/(mol K), $\Delta E_a^{\ddagger}$ = 38.2 $kJmol^{-1.}$ These values were calculated from the temperature-dependent second-order rate constants determined from k_{obs} divided by **[2]** values as provided in (Table TS6) and from the Eyring plot as well as Arrhenius plot in (Figure FS8 and FS9). The Eyring plot indicates a similar ordered transition state in a coordination insertion mechanism reported in the literature. A $\Delta G^{\ddagger}$ value of 40.3 kJ/mol was calculated for the ring-opening polymerization of *rac*-LA catalysed by the catalyst **(2)** at 60 °C.

Table TS2: *rac*-LA polymerizations with time in $CDCl_3$ (1 mL) with different concentration of **catalyst [2].**

S. No	[LA]/[Cat]	Time (min)	Conversion[a] %	[PLA]	[*rac*-LA]$_t$	[LA]$_0$/[LA]	ln ([LA]$_0$/[LA])
1	100/0.5	0	0	0	2	1	0
2	100/0.5	30	6.5	0.13	1.87	1.07	0.07
3	100/0.5	90	13.8	0.276	1.724	1.16	0.15
4	100/0.5	150	19.9	0.398	1.602	1.25	0.22
5	100/0.5	210	25	0.5	1.5	1.33	0.28
6	100/0.5	270	31	0.62	1.38	1.45	0.37
7	100/0.5	330	36	0.72	1.28	1.56	0.44
8	100/1.0	0	0	0	2	1	0
9	100/1.0	30	14.1	0.282	1.718	1.16	0.15
10	100/1.0	90	26.8	0.536	1.464	1.37	0.31
11	100/1.0	150	35	0.7	1.3	1.54	0.43
12	100/1.0	210	41	0.82	1.18	1.69	0.52
13	100/1.0	270	51.2	1.024	0.976	2.05	0.71
14	100/1.0	330	67	1.34	0.66	3.03	1.10
15	100/1.5	0	0	0	2	1	0
16	100/1.5	30	19.5	0.39	1.61	1.24	0.21
17	100/1.5	90	36.6	0.732	1.268	1.58	0.45
18	100/1.5	150	46	0.92	1.08	1.85	0.61
19	100/1.5	210	59.5	1.19	0.81	2.47	0.90
20	100/1.5	270	66.2	1.324	0.676	2.96	1.08
21	100/1.5	330	73	1.46	0.54	3.70	1.31
22	100/2.0	0	0	0	2	1	0
23	100/2.0	30	25.6	0.512	1.488	1.34	0.29
24	100/2.0	90	45.4	0.908	1.092	1.83	0.61
25	100/2.0	150	58.6	1.172	0.828	2.42	0.88
26	100/2.0	210	69	1.38	0.62	3.23	1.17
27	100/2.0	270	76.5	1.53	0.47	4.26	1.45
28	100/2.0	330	83	1.66	0.34	5.88	1.77
29	100/3.0	0	0	0	2	1	0
30	100/3.0	30	35.6	0.712	1.288	1.55	0.44

31	100/3.0	90	63	1.26	0.74	2.70	0.99
32	100/3.0	150	76	1.52	0.48	4.16	1.43
33	100/3.0	210	88	1.76	0.24	8.33	2.12
34	100/3.0	270	93	1.86	0.14	14.28	2.66
35	100/3.0	330	97.5	1.95	0.05	40	3.69

[a]Conversion determined through ^{1}H-NMR spectroscopy, [*rac*-LA]$_0$ is taken 2 for calculation. [PLA]$_0$ is zero at t=0.

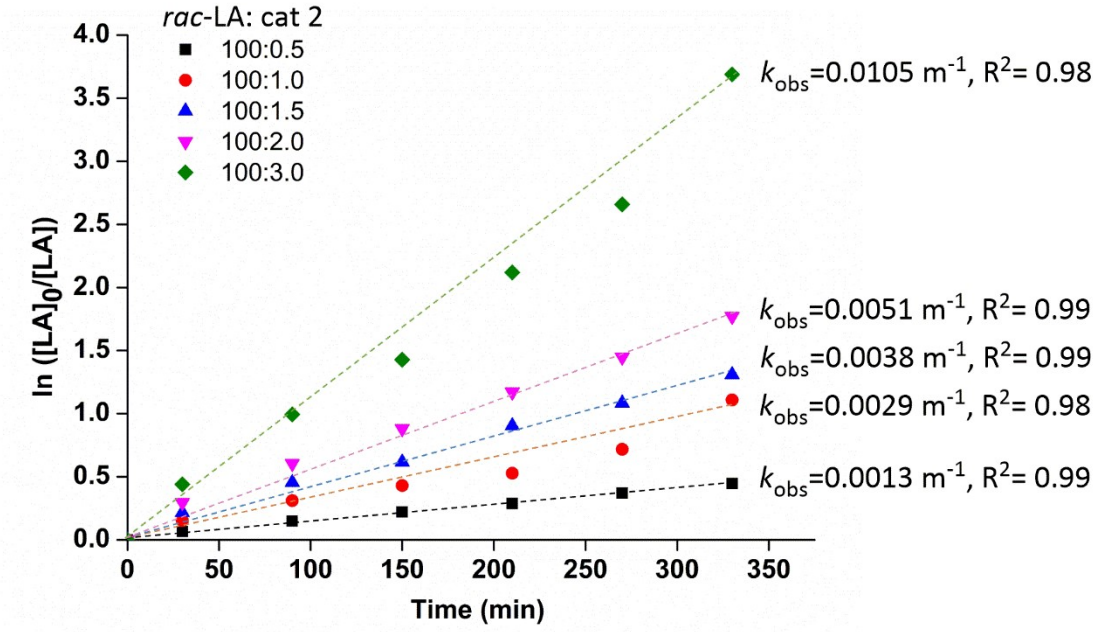

Figure FS4. First-order kinetics plots for *rac*-LA polymerizations (with time) in $CDCl_3$ (0.5 mL) with different concentrations of complex **2** at 60 °C.

Table TS3. Kinetics plots of ln k_{obs} vs ln(2) for the polymerization of *rac*-LA with [LA] = 2.0 M in $CDCl_3$ (1 mL) at 60 °C.

S. No.	**ln [2]**	**ln k_{obs}**
1	-0.69	-6.65
2	0	-5.84
3	0.41	-5.57
4	0.69	-5.28
5	1.09	-4.56

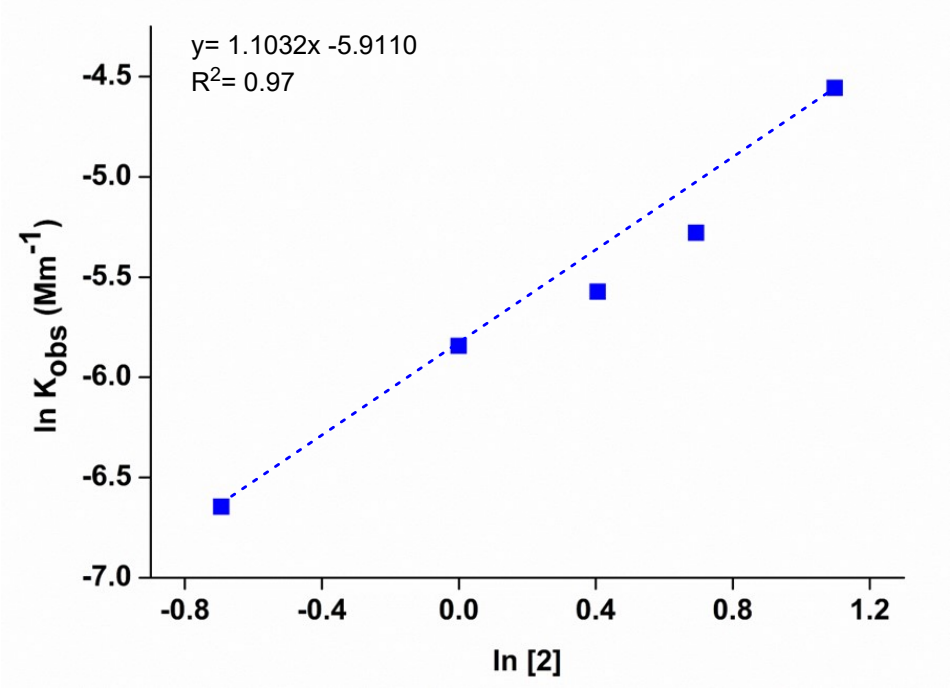

Figure FS5. Kinetics plots of K_{obs} versus in ln[κ^2-{NHI^{Dipp}P(Ph)NDipp}Cs] for the polymerization of *rac*-LA with [LA] = 2.0 M in $CDCl_3$ (0.5 mL) at 60 ^oC.

Table TS4: Kinetics plots of k_{obs} vs cat (2) for the polymerization of *rac*-LA with [LA] = 2.0 M in $CDCl_3$ (1 mL) at 60 ^0C.

S. No.	[2] (M)	K_{obs} (Mm^{-1})
1	0.5	0.0013
2	1	0.0029
3	1.5	0.0038
4	2	0.0051
5	3	0.0105

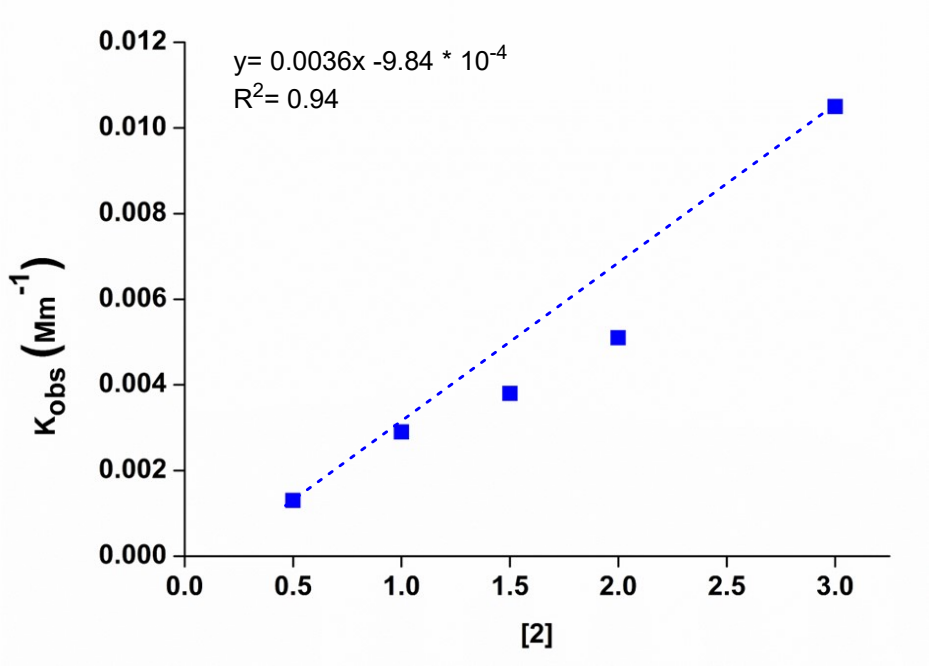

Figure FS6: Kinetics plots of k_{obs} vs cat [2] for the polymerization of *rac*-LA with [LA] = 2.0 M in $CDCl_3$ (0.5 mL) at 60 ^{0}C.

Rate of the reaction = $-d[LA]/dt = (1.1)\,[LA]^1[\kappa^2\text{-}\{NHI^{Dipp}P(Ph)NDipp\}Cs]^1$

Eyring Equation:

$$\ln \frac{k}{T} = \frac{-\Delta H^{\ddagger}}{R} \cdot \frac{1}{T} + \ln \frac{k_B}{h} + \frac{\Delta S^{\ddagger}}{R}$$

Arrhenius Equation:

$$\ln k = \frac{-E_a}{R}\left(\frac{1}{T}\right) + \ln A$$

Where,

- k_B is the Boltzmann's constant (1.381 x 10^{-23} J/K)
- T is the absolute temperature in Kelvin (K)
- h is Planck's constant (6.626 x 10^{-34} Js)
- $\Delta H^{\ddagger}$ is **enthalpy of activation** (J/(mol K)
- $\Delta S^{\ddagger}$ is **entropy of activation** (J/(mol K)
- $\Delta E_a^{\ddagger}$ is activation energy (J/(mol K)
- $\Delta G^{\ddagger}$ is Gibbs energy of activation (J/mol)
- R is Gas constant (8.314 J/K mol)

First order kinetics plots for *rac*- LA polymerizations with time in $CDCl_3$ (0.5 mL) with different range of temperatures catalysed by **2** is shown in Figure FS10. The activation parameters for the ROP or *rac*-LA in $CDCl_3$ were found to be $\Delta H^{\ddagger}$= 36.6 kJ/mol K and $\Delta S^{\ddagger}$= -11.2 J/(mol K), $\Delta E_a^{\ddagger}$ = 38.2 $kJmol^{-1}$. These values were calculated from the temperature-dependent second-order rate constants determined from k_{obs} divided by **[2]** values as provided in (Table TS6) and from the Eyring plot as well as Arrhenius plot in (Figure FS11, FS12). The Eyring plot (Figure FS11) indicates a similar ordered transition state in a coordination insertion mechanism reported in the literature. A $\Delta G^{\ddagger}$ value of 40.3 kJ/mol was calculated for the ring-opening polymerization of *rac*-LA catalysed by the catalyst **(2)** at 60 °C.

Table TS5. *rac*-LA polymerizations with time in $CDCl_3$ (0.5 mL) at different temperatures of **catalyst [2].** (*rac*-LA:2= 100:2)

S. No	T (K)	Time (min)	Conversion %	[PLA]	[*rac*-LA]^t	$[LA]_0/[LA]$	$\ln([LA]_0/[LA])$
1	313	0	0	0	2	1	0
2	313	30	14.3	0.28	1.71	1.17	0.15
3	313	90	25.5	0.51	1.49	1.34	0.29
4	313	150	34.6	0.69	1.31	1.53	0.42
5	313	210	44.7	0.89	1.11	1.81	0.59
6	313	270	50.5	1.01	0.99	2.02	0.70
7	323	0	0	0	2	1	0
8	323	30	21.4	0.42	1.572	1.27	0.24
9	323	90	38	0.76	1.24	1.61	0.48
10	323	150	47.6	0.95	1.05	1.91	0.65
11	323	210	59.5	1.19	0.81	2.46	0.90
12	323	270	69	1.38	0.62	3.23	1.17
13	333	0	0	0	2	1	0
14	333	30	25.6	0.51	1.49	1.34	0.29
15	333	90	45.4	0.90	1.09	1.83	0.61
16	333	150	58.6	1.17	0.83	2.42	0.88
17	333	210	69	1.38	0.62	3.23	1.17
18	333	270	76.5	1.53	0.47	4.26	1.45
19	343	0	0	0	2	1	0

20	343	30	36	0.72	1.28	1.56	0.45
21	343	90	60.5	1.21	0.79	2.53	0.93
22	343	150	75.2	1.50	0.49	4.03	1.39
23	343	210	82	1.64	0.36	5.55	1.71
24	343	270	91	1.82	0.18	11.11	2.40
25	353	0	0	0	2	1	0
26	353	30	51	1.02	0.98	2.04	0.71
27	353	90	79.5	1.59	0.41	4.87	1.58
28	353	150	89.3	1.78	0.21	9.34	2.23
29	353	210	93	1.92	0.08	25	3.22
30	353	270	99	1.98	0.02	100	4.61

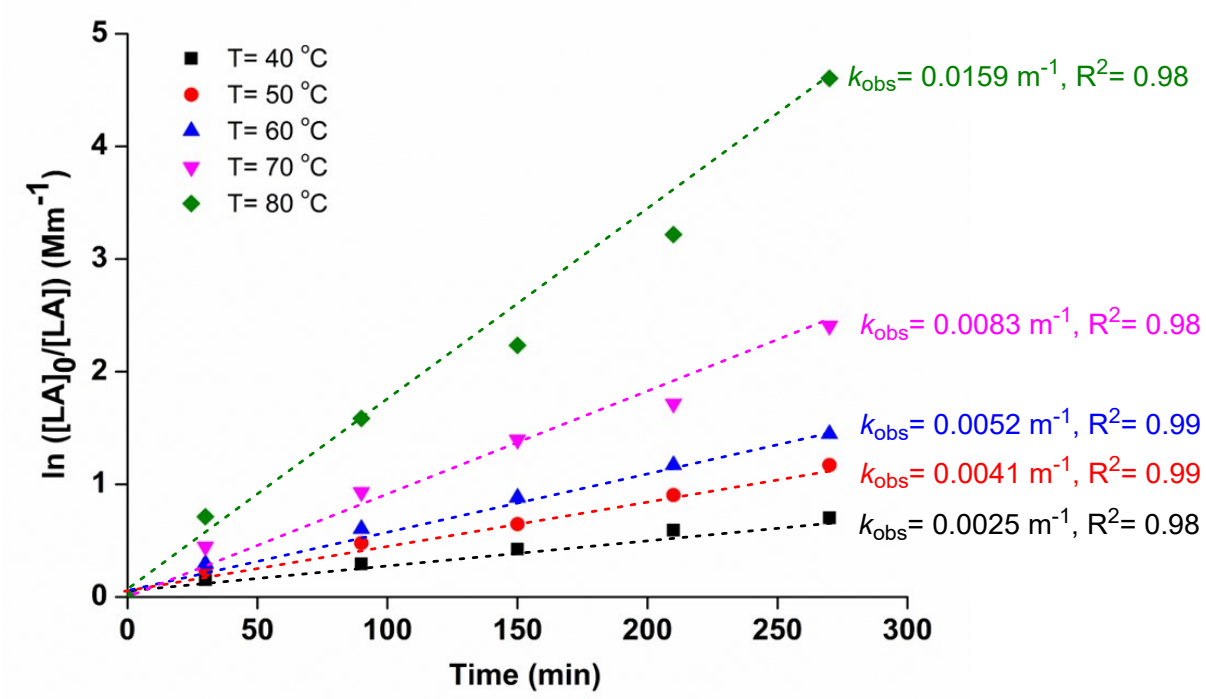

Figure FS7. First order kinetics plots for *rac* LA polymerizations with time in $CDCl_3$ (0.5 mL) with different temperature catalysed by [κ^2-{NHI^{Dipp}P(Ph)NDipp}Cs] (**2**).

Table TS6. Table for Eyring plot and Arrhenius plot of ln(k_{obs}/T) vs (1/T) catalysed by [κ^2-{NHI^{Dipp}P(Ph)NDipp}Cs] (**2**) as catalyst for the polymerization of *rac*-LA with [LA] = 2.0 M in $CDCl_3$ (0.5 mL).

Entry	K_{obs}	1/T	ln k_{obs}/T
1	0.0025	0.0032	-5.99
2	0.0041	0.0031	-5.49
3	0.0052	0.0030	-5.26
4	0.0083	0.0029	-4.79
5	0.0159	0.0028	-4.14

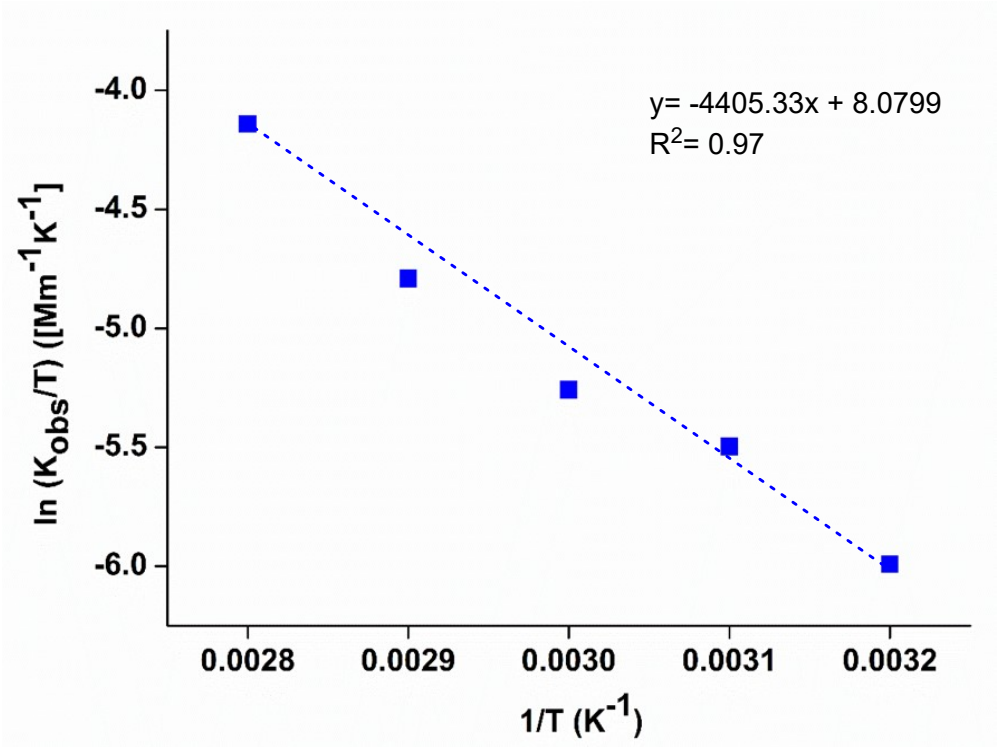

Figure FS8. Eyring plot of ln(k_{obs} /T) ($Mm^{-1}K^{-1}$) vs (1/T) (K^{-1}) for [κ^2-{NHI^{Dipp}P(Ph)NDipp}Cs] (**2**) cat for the polymerization of *rac*-LA with [LA] = 2.0 M in $CDCl_3$ (0.5 mL) of *rac*-LA (0.01 M) with [LA] = 2.0 M in $CDCl_3$ (1 mL). $\Delta H^{\ddagger}$ = 36.6 kJ mol^{-1} $\Delta S^{\ddagger}$ = -11.2 J $mol^{-1}K^{-1}$ ($CDCl_3$).

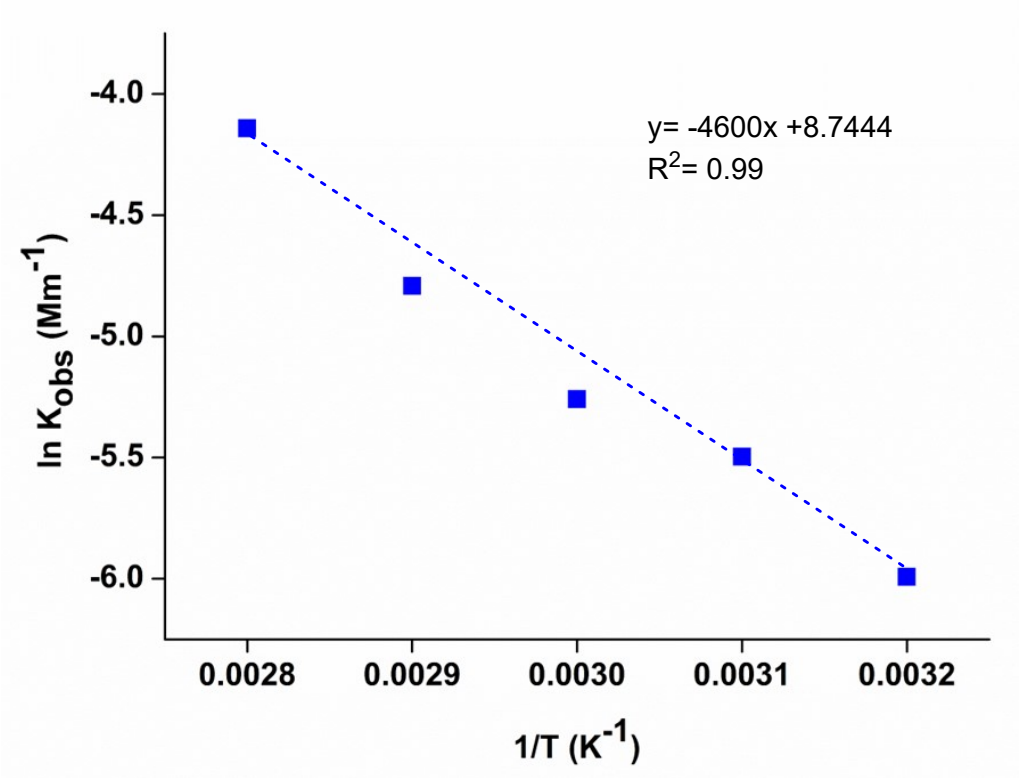

Figure FS9. Arrhenius plots of ln(k_{obs}) (Mm^{-1}) vs (1/T) (K^{-1}) for [κ²-{NHI^{Dipp}P(Ph)NDipp}Cs] (**2**) catalyst for the polymerization of *rac*-LA with [LA] = 2.0 M in $CDCl_3$ (0.5 mL) of *rac*-LA (0.01 M) with [LA] = 2.0 M in $CDCl_3$ (0.5 mL), E_a = 38.2 $kJmol^{-1}$

Conversion through ^{1}H NMR spectrum at different time intervals and different concentrations of catalyst 2 in $CDCl_3$

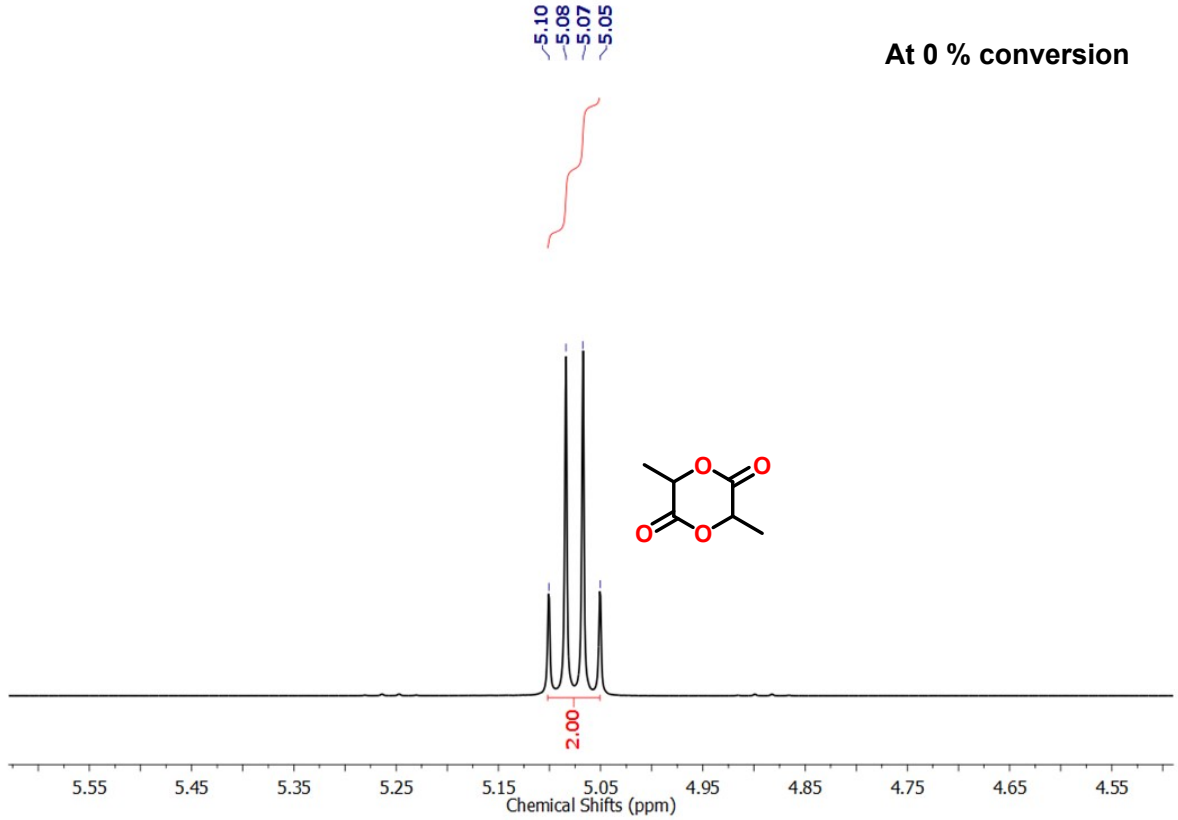

Figure FS10. ^{1}H NMR spectrum of *rac*-LA polymerization using catalyst **2** (0.5 mol%), $CDCl_3$ after 1 min at 60 ˚C on 0% conversion [Table TS2, Entry 1].

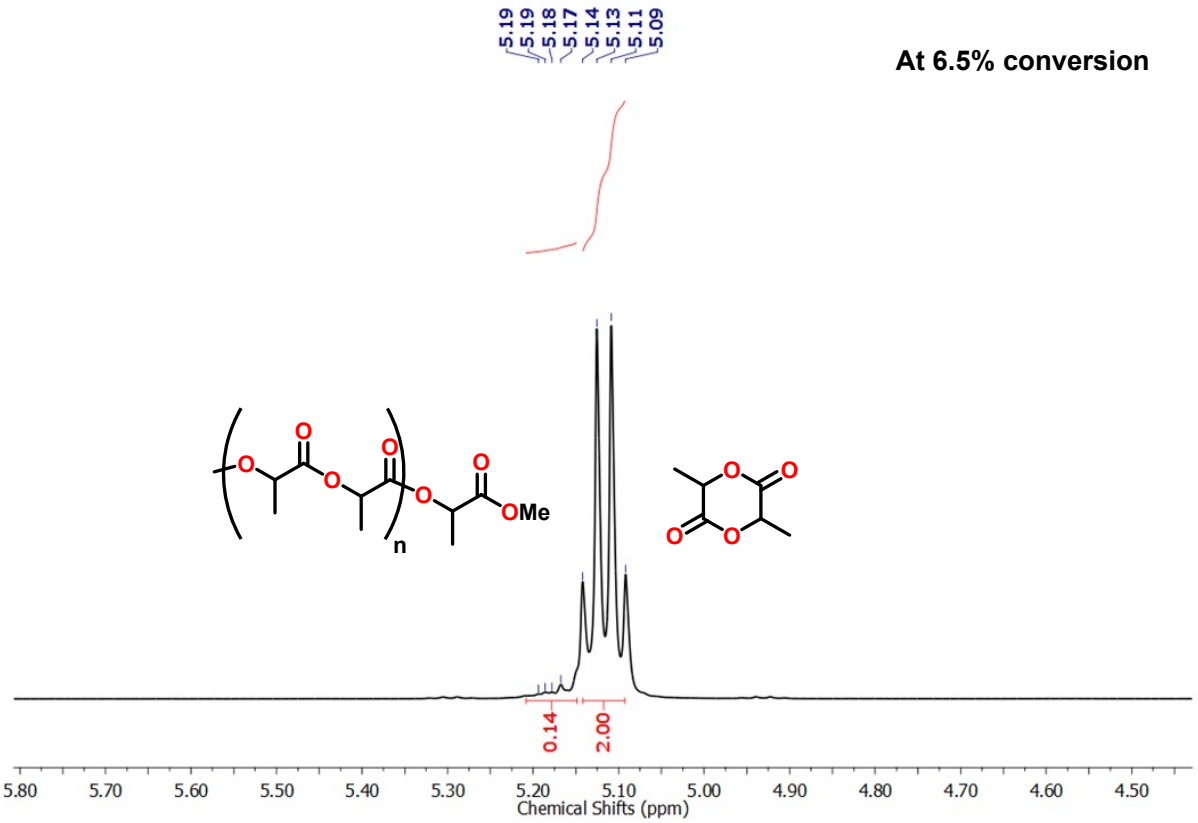

Figure FS11. ^{1}H NMR spectrum of *rac*-LA polymerization using catalyst **2** (0.5 mol%), $CDCl_3$ after 30 min at 60 ˚C on 6.5% conversion [Table TS2, Entry 2].

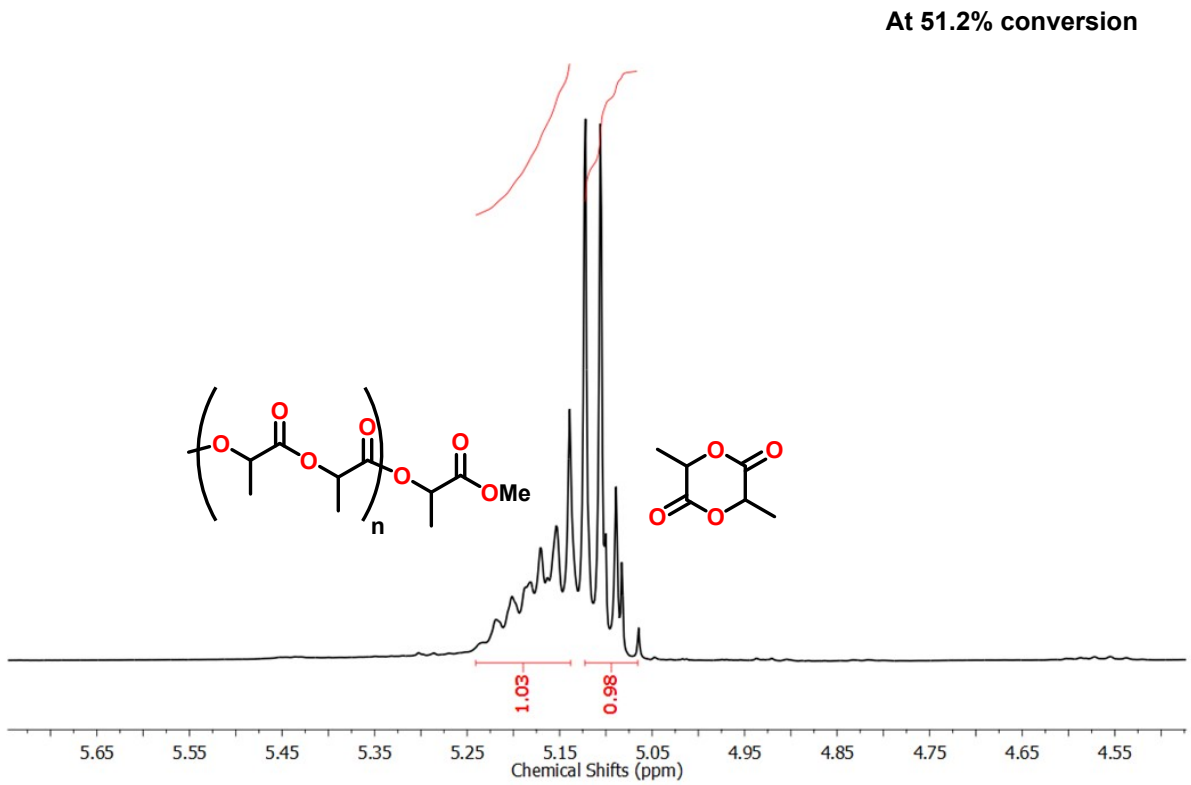

Figure FS12. ^{1}H NMR spectrum of *rac*-LA polymerization using catalyst **2** (1.0 mol%), $CDCl_3$ after 270 min at 60 ˚C on 51.2% conversion [Table TS2, Entry 13].

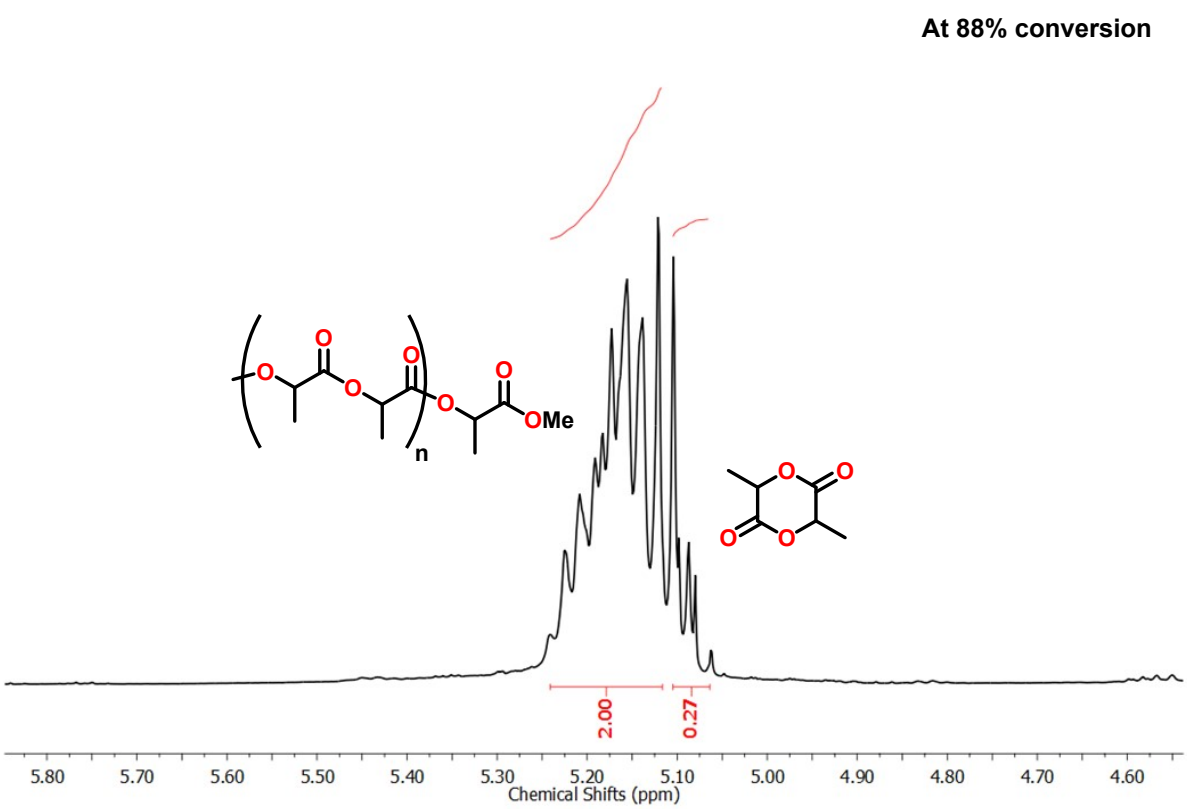

Figure FS13. ^{1}H NMR spectrum of *rac*-LA polymerization using catalyst **2** (2.5 mol%), $CDCl_3$ after 210 min at 60 ˚C on 88% conversion [Table TS2, Entry 33].

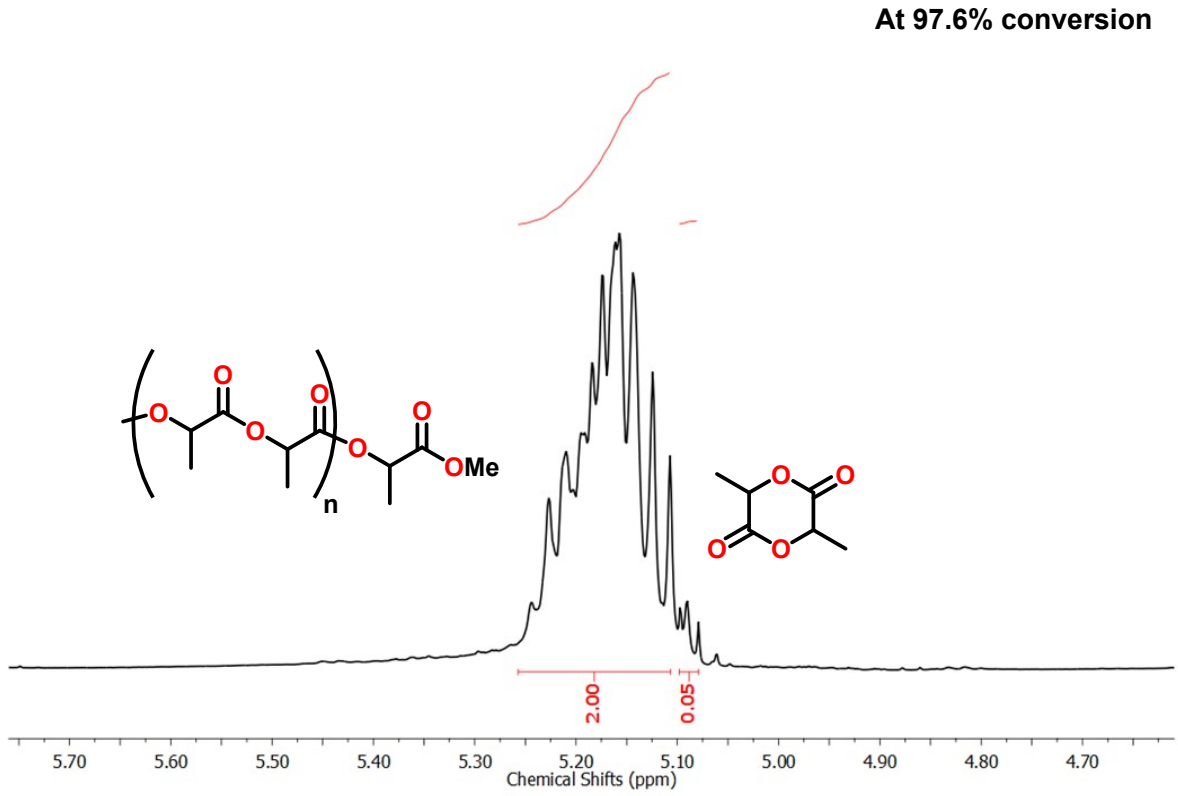

Figure FS14. ^{1}H NMR spectrum of *rac*-LA polymerization using catalyst **2** (2.5 mol%), $CDCl_3$ after 330 min at 60 ˚C on 97.6% conversion [Table TS2, Entry 35].

Kinetics study in presence of benzyl alcohol as an external initiator

[κ^2-{NHI^{Dipp}P(Ph)NDipp}Cs]/(2) as a catalyst in presence of BnOH: A typical kinetics study was performed to establish the reaction order with respect to monomer *rac*–LA, [κ^2-{NHI^{Dipp}P(Ph)NDipp}Cs] (**2**) and benzyl alcohol. For LA polymerization, *rac*–LA (0.1 g, 0.6944 mmol) and benzyl alcohol (0.0069 mmol) was added to a solution of **2** (0.007, 0.01, 0.02, 0.03, 0.04 M) in $CDCl_3$ (0.5 mL), respectively. The solution was set in the NMR tube at 60 ˚C. After that at the indicated time intervals, the tube was analyzed by ^{1}H NMR spectroscopy. The *rac*-LA concentration [LA] was determined by integrating the quartet methine peak of LA at 5.01 ppm and the broad singlet methine peak at 5.09-5.20 ppm. As expected, plots of $[LA]_0/[LA]$ vs. time for a wide range of **2** are linear indicating the usual first order dependence on monomer concentration (Figure FS18). Thus, the rate expression can be written as

$$-d[LA]/dt = k[La]^1[\kappa^2\text{-}\{NHI^{Dipp}P(Ph)NDipp\}Cs]^x = k_{obs}[LA]^1$$

$$\text{where } k_{obs} = k\,[\kappa^2\text{-}\{NHI^{Dipp}P(Ph)NDipp\}Cs]^x$$

A plot of ln(k_{obs}) vs. ln[κ^2-{NHI^{Dipp}P(Ph)NDipp}Cs]^x (Figure FS18, Table TS7) is linear, indicating the order of [κ^2-{NHI^{Dipp}P(Ph)NDipp}Cs] is (x = 1.01 or 1). From the kinetics data, it can be clearly demonstrated that there was almost no change in values for rate constant for the ROP of *rac*-LA catalysed by **2** in presence of benzyl alcohol (Figure FS19).

Table TS7. *rac*-LA polymerizations with time in $CDCl_3$ (0.5 mL) with different concentration of catalyst **2 (M)** in the presence of BnOH.

S. No	[LA]/[2]/ BnOH	Time (min)	Conversion %	[PLA]	[*rac*-LA]^t	$[LA]_0/[LA]$	ln ($[LA]_0/[LA]$)
1	100/0.5	0	0	0	2	1	0
2	100/0.5	60	35	0.15	1.85	1.079	0.076
3	100/0.5	120	56	0.29	1.70	1.17	0.16
4	100/0.5	180	73	0.42	1.58	1.26	0.23
5	100/0.5	240	80	0.55	1.45	1.38	0.32
6	100/1.0	0	0	0.66	1.34	1.49	0.40
7	100/1.0	60	42	0.74	1.26	1.58	0.46
8	100/1.0	120	64	0	2	1	0
9	100/1.0	180	79	0.31	1.69	1.18	0.16
10	100/1.0	240	88	0.56	1.44	1.38	0.32
11	100/1.5	0	0	0.71	1.28	1.55	0.44
12	100/1.5	60	51	0.82	1.18	1.70	0.53
13	100/1.5	120	70	1.05	0.95	2.11	0.74
14	100/1.5	180	89	1.23	0.77	2.59	0.95
15	100/1.5	240	95	0	2	1	0
16	100/2.0	0	0	0.47	1.53	1.31	0.27
17	100/2.0	60	59	0.83	1.17	1.70	0.54
18	100/2.0	120	76	1.02	0.98	2.04	0.71
19	100/2.0	180	92	1.24	0.76	2.63	0.97
20	100/2.0	240	97	1.4	0.6	3.33	1.20
21	100/2.5	0	0	1.63	0.37	5.41	1.69
22	100/2.5	60	63	0	2	1	0
23	100/2.5	120	82	0.51	1.488	1.34	0.29

24	100/2.5	180	91	0.93	1.07	1.86	0.63
25	100/2.5	240	99	1.22	0.78	2.57	0.94
26	100/2.0/1	210	71.3	1.43	0.57	3.48	1.25
27	100/2.0/1	270	78.7	1.57	0.43	4.69	1.55
28	100/2.0/1	330	85	1.7	0.3	6.66	1.89
29	100/2.5/1	0	0	0	2	1	0
30	100/2.5/1	30	37	0.74	1.26	1.59	0.46
31	100/2.5/1	90	59.5	1.19	0.81	2.47	0.90
32	100/2.5/1	150	73.2	1.46	0.536	3.73	1.32
33	100/2.5/1	210	80.5	1.61	0.39	5.13	1.63
34	100/2.5/1	270	91	1.82	0.18	11.11	2.41
35	100/2.5/1	330	95	1.9	0.1	20	2.99

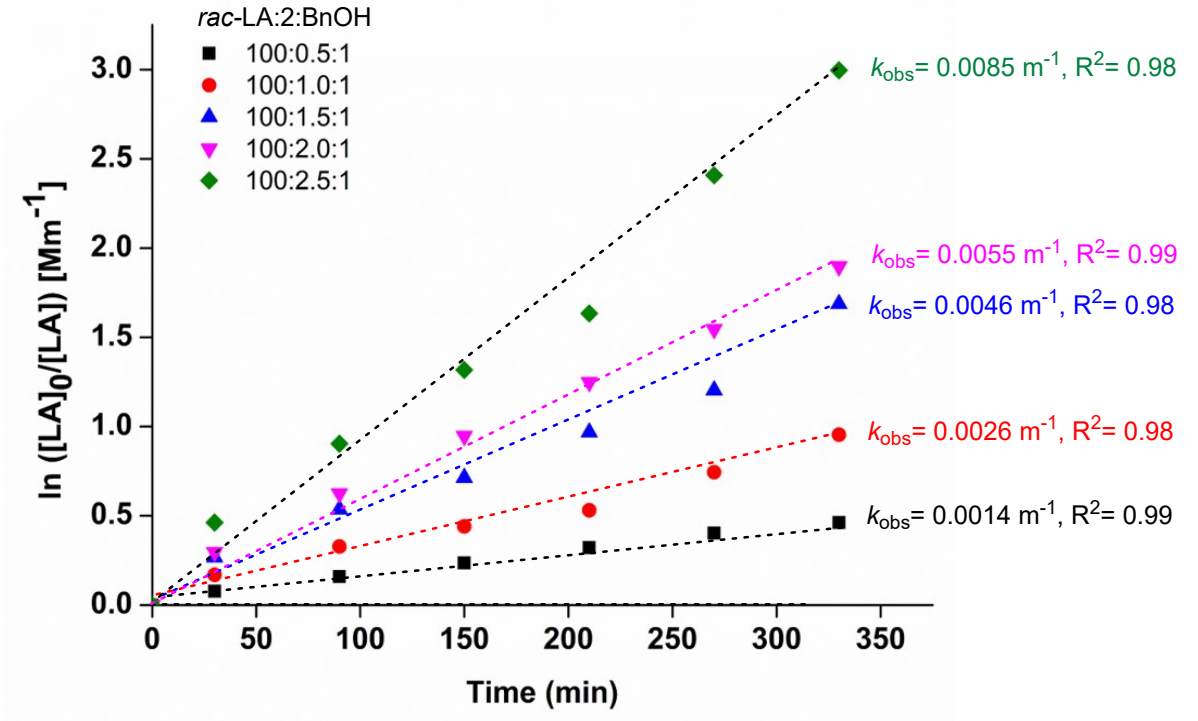

Figure FS15. First order kinetics plots for *rac*- LA polymerizations with time in $CDCl_3$ (0.5 mL) with different concentration of [κ²-{NHI^{Dipp}P(Ph)NDipp}Cs] (**2**) at 60 ˚C having *rac*– LA (0.1 g, 0.694 mmol) and benzyl alcohol (0.007 mmol).

Table TS8. Kinetics plots of ln k_{obs} vs ln (2) for the polymerization of *rac*-LA with [LA] = 2.0 M in $CDCl_3$ (0.5 mL) at 60 ^{0}C in the presence of BnOH.

S. No.	ln [2] (cat)	ln K_{obs}
1	-0.69	-6.57
2	0	-5.95
3	0.41	-5.38
4	0.69	-5.20
5	1.09	-4.77

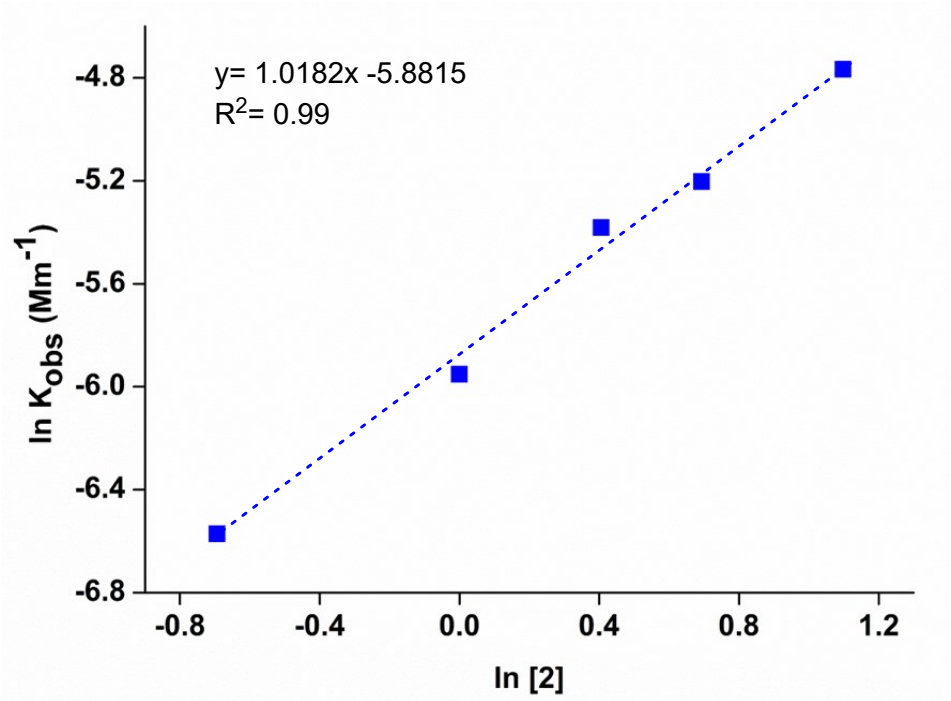

Figure FS16: Kinetics plots of lnk_{obs} vs ln(**2**) for the polymerization of *rac*-LA with [LA] = 2.0 M and benzyl alcohol (0.007 mmol) in $CDCl_3$ (0.5 mL) at 60 ˚C.

Table TS9. Kinetics plots of k_{obs} vs cat (2) for the polymerization of *rac*-LA with [LA] = 2.0 M in $CDCl_3$ (0.5 mL) at 60 ^{0}C in the presence of BnOH.

S. No.	[2] (cat)	K_{obs}
1	0.5	0.0014
2	1	0.0026
3	1.5	0.0046
4	2	0.0055
5	3	0.0085

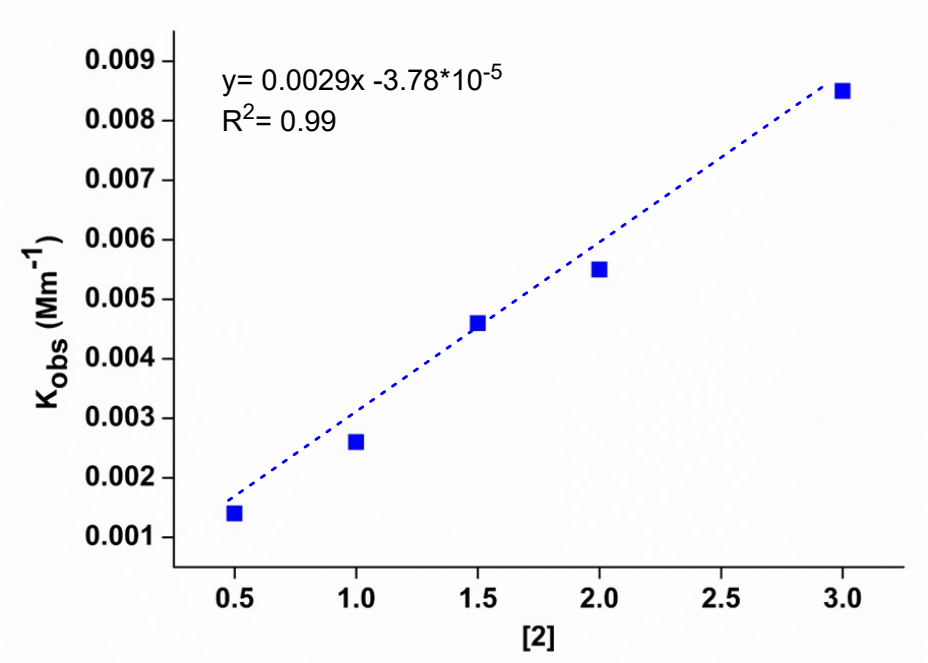

Figure FS17: Kinetics plots of k_{obs} vs (**2**) for the polymerization of *rac*-LA with [LA] = 2.0 M and benzyl alcohol (0.007 mmol) in $CDCl_3$ (0.5 mL) at 60 ˚C.

Further, reactions were performed by varying the concentration of BnOH (0.01, 0.02, 0.04, 0.07, 0.1 M) and keeping the catalyst **2** concentration (0.01 M) and *rac*-LA (0.1 g, 0.694 mmol) constant. The plot of $[LA]_0/[LA]$ vs. time for a wide range of **2** are linear indicating the usual first-order dependence on monomer concentration (Figure FS20) but in all cases the value of rate constant k_{obs} remain same. This lack of dependence on benzyl alcohol concentration confirms its zero-order contribution to the rate law (Figure FS21). Thus, the kinetics study proved that polymerization reaction does not depends on external initiator and our catalyst itself act as an initiator for ROP of *rac*- LA.

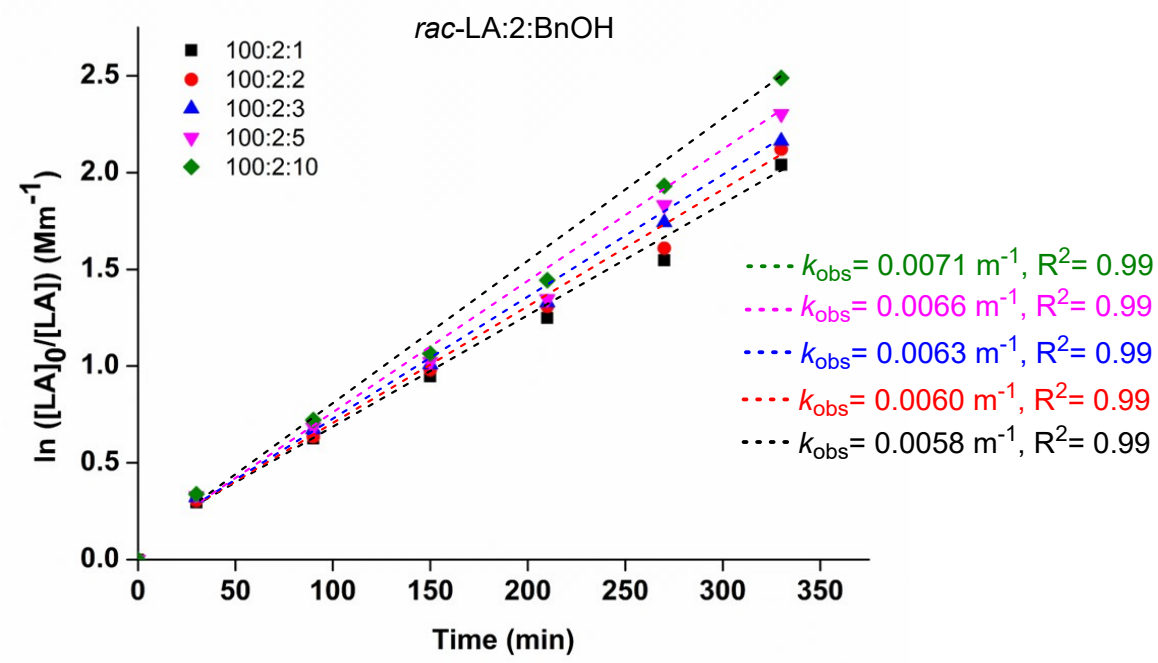

Figure FS18. First order kinetics plots for *rac*- LA polymerizations with time in $CDCl_3$ (0.5 mL) with different concentration of BnOH at 60 ˚C having *rac*–LA (0.1 g, 0.694 mmol) and (**2**) as catalyst (0.0138 mmol).

Table TS10: Kinetics plots of ln k_{obs} vs ln (BnOH) for the polymerization of *rac*-LA with [LA] = 2.0 M in $CDCl_3$ (0.5 mL) at 60 ^{0}C.

S. No.	ln [BnOH]	ln K_{obs}
1	0	-5.14
2	0.69	-5.11
3	1.09	-5.06
4	1.60	-5.02
5	2.30	-4.95

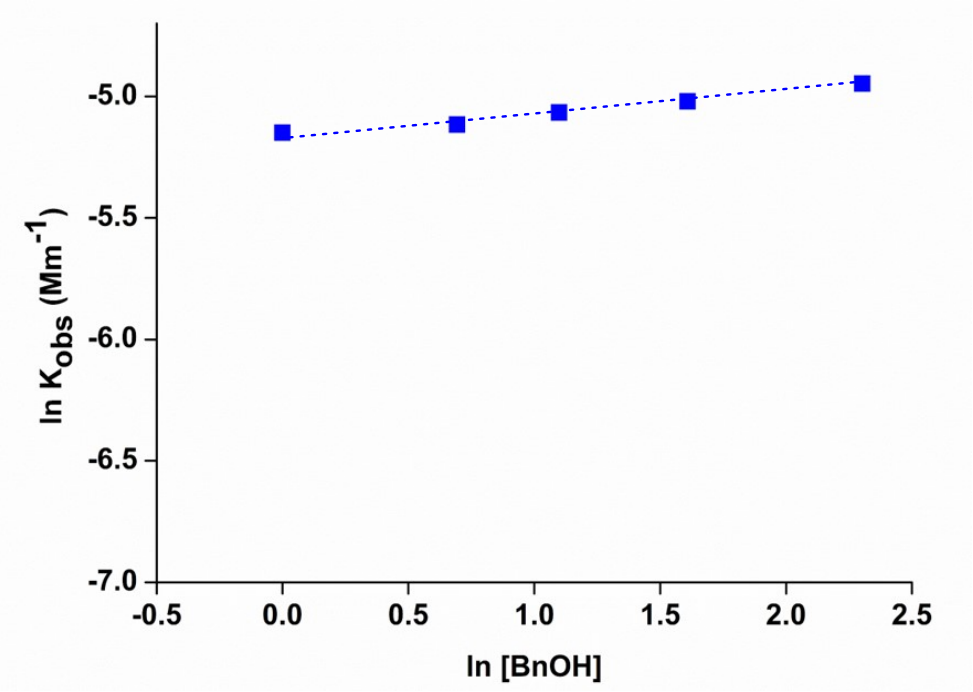

Figure FS19. Kinetics plots of ln k_{obs} vs ln[benzyl alcohol] for the polymerization of *rac*-LA (0.1 g, 0.694 mmol) and (**2**) as catalyst (0.0138 mmol).

Cha*rac*terisation of PLA

A typical polymerization procedure is exemplified by the synthesis of poly(*rac*-lactide) at ambient temperature (TableTS12). *Rac*-LA (0.288 g, 2.0 mmol) was added to a solution of **2** (0.008 g, 0.01 mmol) in toluene (5 mL). After the desired reaction time, the monomer was converted into polymer, so the reaction was then quenched by the addition of a drop of 2 N HCl and methanol. Then solution was concentrated in vacuum and polymer was recrystallized with dichloromethane and hexane. The final polymer was filtered and dried under vacuum to constant weight.

Table TS11: *rac*-lactide polymerization using catalyst 2[a].

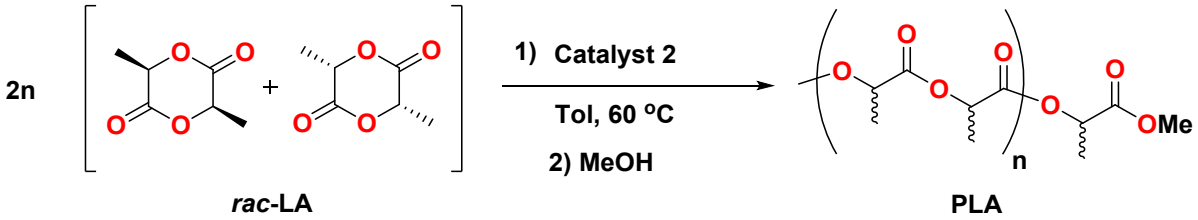

Entry	M:1	Time (h:m)	Conv[b]	Yield[c]	M_{ntheo} (kDa)[d]	M_{nexp}[e] (kDa)	PDI	P_i[h]
1	100	06:00	98	99	14.3	16.1	1.3	0.81
2[f]	100	06:00	58	65	8.5	6.9	1.0	0.61
3[g]	100	06:00	90	89	13.1	10.9	1.1	0.71
4	200	06:00	97	95	28.1	23.5	1.4	0.79
5	300	06:00	98	96	42.5	45.5	1.2	0.78
6	400	06:00	95	93	54.9	52.1	1.1	0.80
7	500	06:00	98	97	70.7	74.8	1.3	0.76

[a]In toluene, [Catalyst] = 1 mM, [b]Conversions were determined by ^{1}H NMR spectroscopy. [c]Isolated yield. [d]$M_{n\,(theo)}$ = molecular weight of chain-end + 144 gmol^{-1} ×(M:1) × conversion. [e]In THF (2 mg mL^{-1}) and molecular weights were determined by GPC-LLS (flow rate ¼ 0.5 mL min^{-1}). [f]In THF as a solvent. Universal calibration was carried out with polystyrene standards, laser light scattering detector data, and concentration detector. Each experiment is duplicated to ensure precision. [g]In presence of initiator (BnOH).[h]P_i determined by analysis of all the tetrad signals in the methine region of the homonuclear-decoupled ^{1}H NMR spectrum.

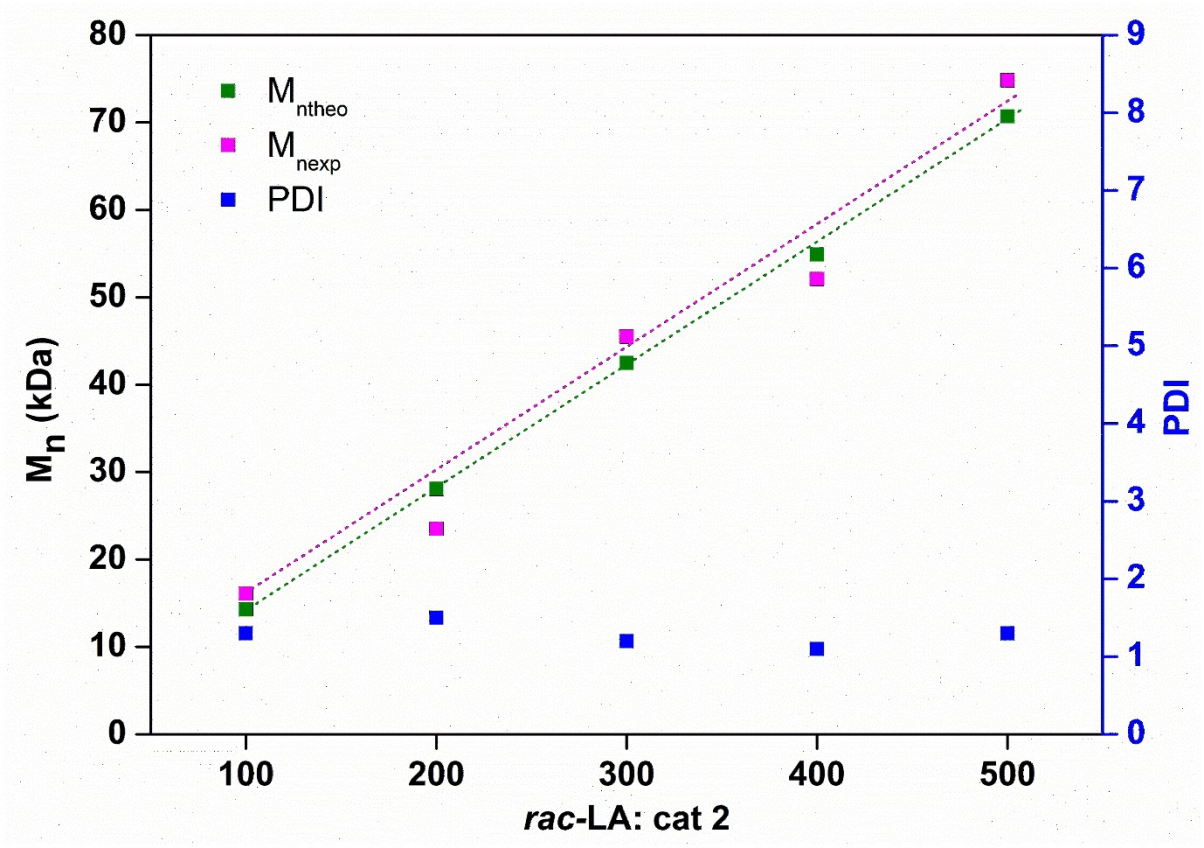

Figure FS20. Plot of theoretical, experimental M_n and molecular weight distribution of PLA as functions of molar equivalent of *rac*-LA with respect to catalyst **2** (M_n = number average molecular weight, PDI = polydispersity index).

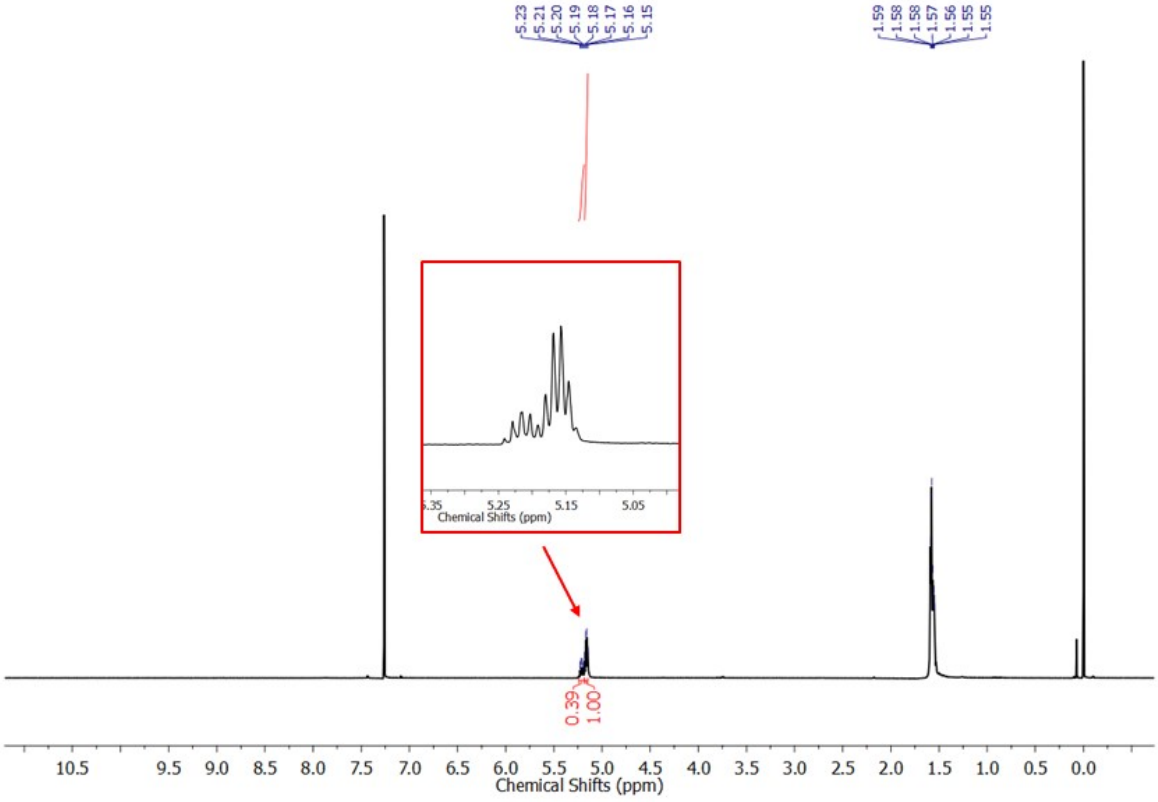

Figure FS21: ^{1}H NMR spectrum ($CDCl_3$, 25 °C) of polymerization solution sample for conversion calculation in Table TS11, Entry 1.

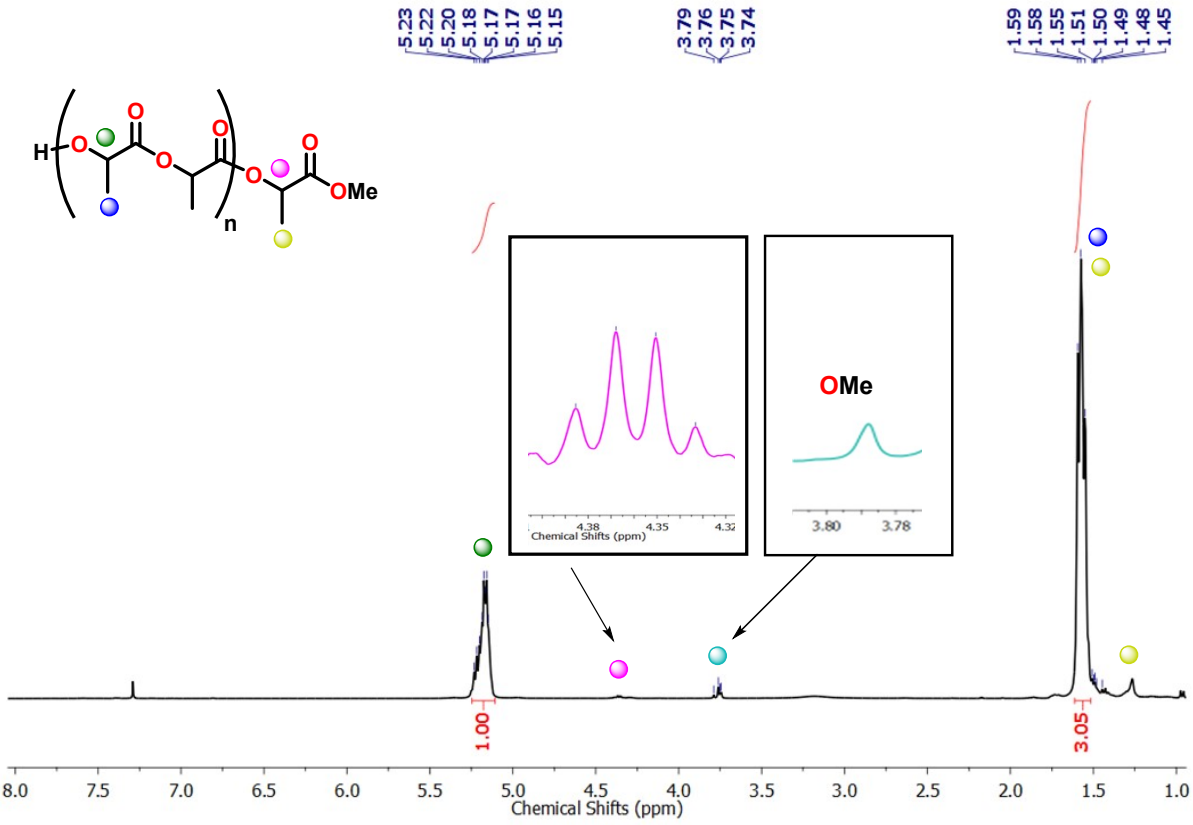

Figure FS22. ^{1}H-NMR spectra of PLA obtained (Entry 1, Table TS11)

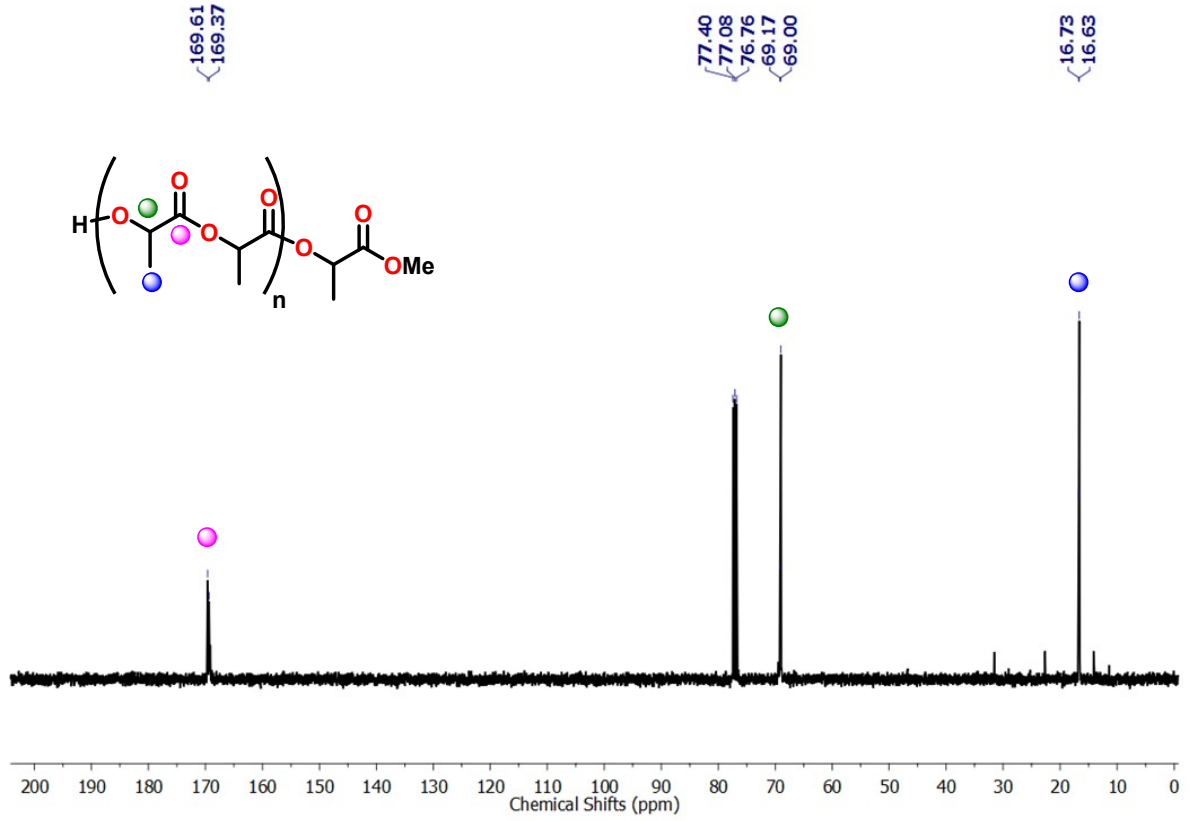

Figure FS23. ^{13}C-NMR spectra of PLA obtained (Entry 1, Table TS11)

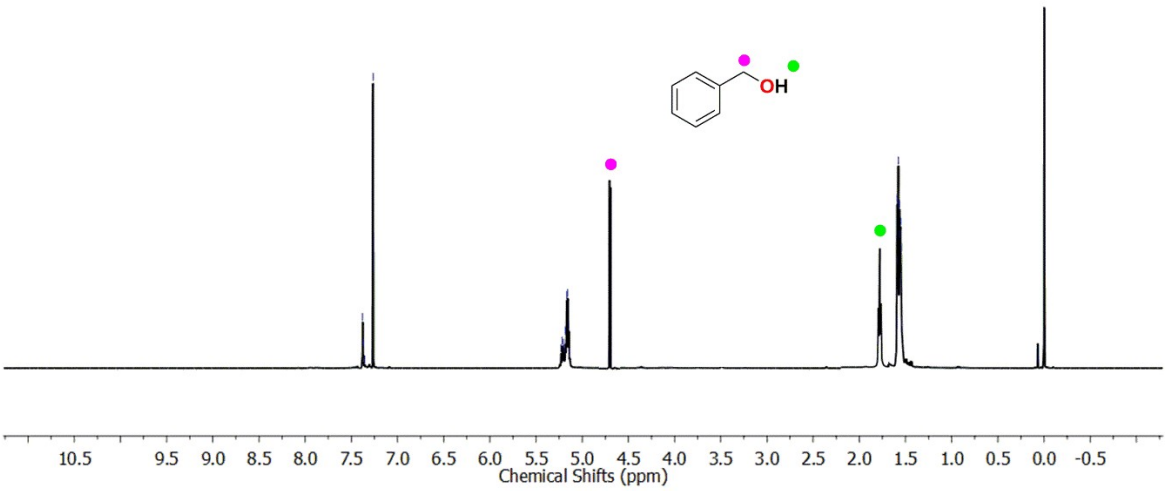

Figure FS24: ^{1}H NMR spectrum of an aliquot from the crude mixture (BnOH, cat **2**, *rac*-LA)

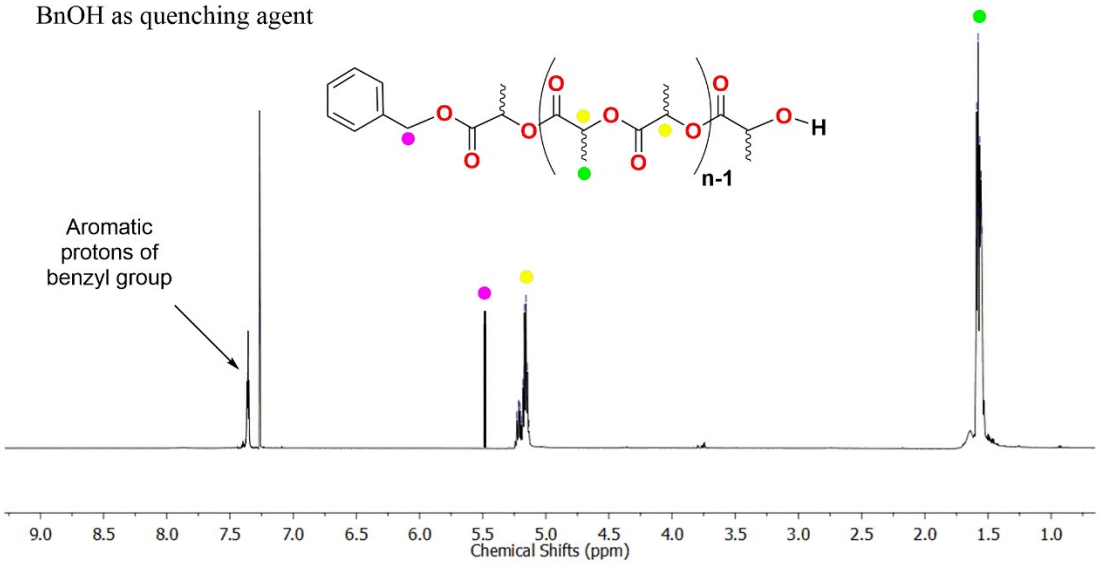

Figure FS25: ^{1}H NMR spectrum of PLA quenched by BnOH.

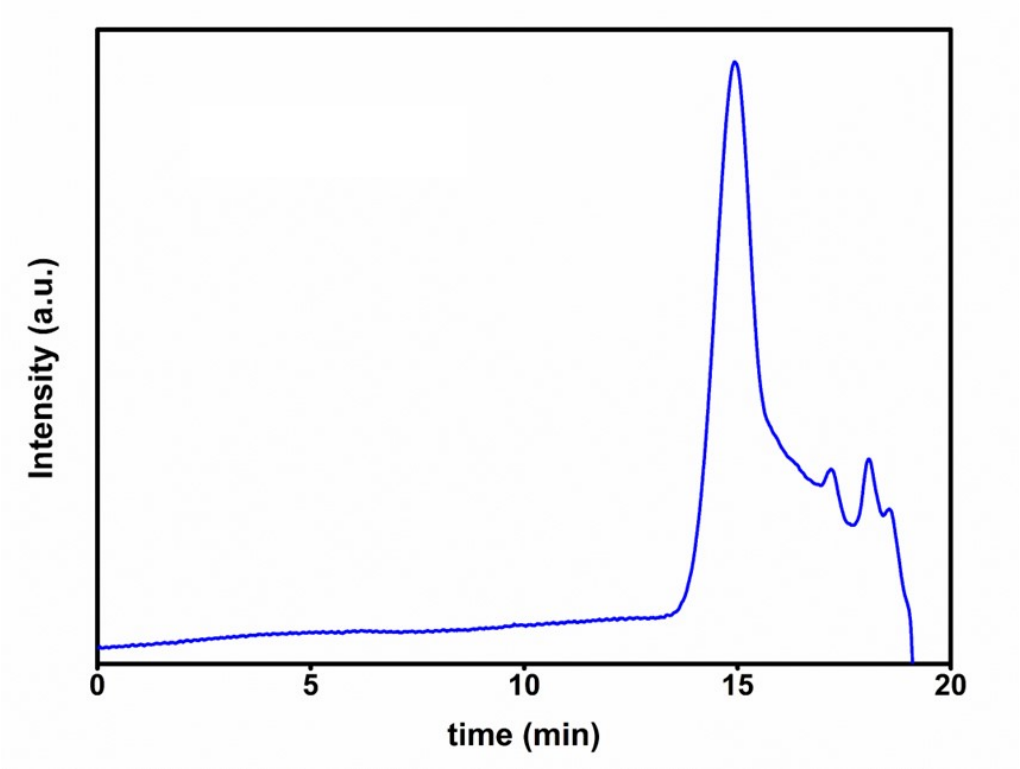

Figure FS26. GPC profile of sample of PLA $M_{n\ (exp)}$= 52.1 kDa, PDI= 1.1 [Entry 6 in Table TS11]

Calculation of P_r / P_m Values

For ROP of lactide, there have been various well-known mechanisms such as anionic, pseudo-anionic (general base catalysis), coordination–insertion ROP and monomer-activated mechanisms. Stereocontrol polymers can be achieved via two different mechanisms, one is chain end control and other is enantiomorphic site control. In case of chain end-controlled mechanism, the chirality of the propagating chain end bound to the catalyst will determine the chirality of the next monomer to be inserted which is associated with hindered catalyst systems so that chirality of the polymer depend on the chirality of the monomer. Whereas in enantiomorphic site control, chirality of the polymer usually depends on the chirality of the catalyst and not the chain end which determines the chirality of the next insertion. Alkali and alkaline earth metal-based catalysts are usually considered to be following stereo control in polymerization of *rac*-lactide via a chain end control mechanism and a Bernoullian statistics mode was usually employed to calculate P_m/P_r values. P_m/P_r is the probability of mesomeric /*rac*emic linkages between monomer units determined from the methine region of the homonuclear decoupled ^{1}H NMR spectrum. P_r can also be expressed in terms of the enchainment rate constants: $P_r = k_{R/SS}/(k_{R/SS} + k_{R/RR}) = k_{S/RR}/(k_{S/RR}+k_{S/SS})$. The expressions for

the tetrad concentrations in terms of P_r, assuming Bernoullian statistics and the absence of transesterification, are as follows:

Table TS13. Tetrad Probabilities Based on Bernoullian Statistics

tetrad Probability(*rac*-lactide)

[*mmm*] $P_m^2 + (1-P_m)P_m/2$

[*mmr*] $(1-P_m)P_m/2$

[*rmm*] $(1-P_m)P_m/2$

[*rmr*] $(1-P_m)^2/2$

[*rrr*] 0

[*rrm*] 0

[*mrr*] 0

[*mrm*] $[(1-P_m)^2 + (1-P_m)P_m]/2$

Most stereoselective ROP of *rac*-lactide in literatures involve only one single-site catalyst and the calculation of P_m / P_r usually use single-state statistic model even if in the case when *rac*-catalysts were used in ROP of *rac*-lactide.

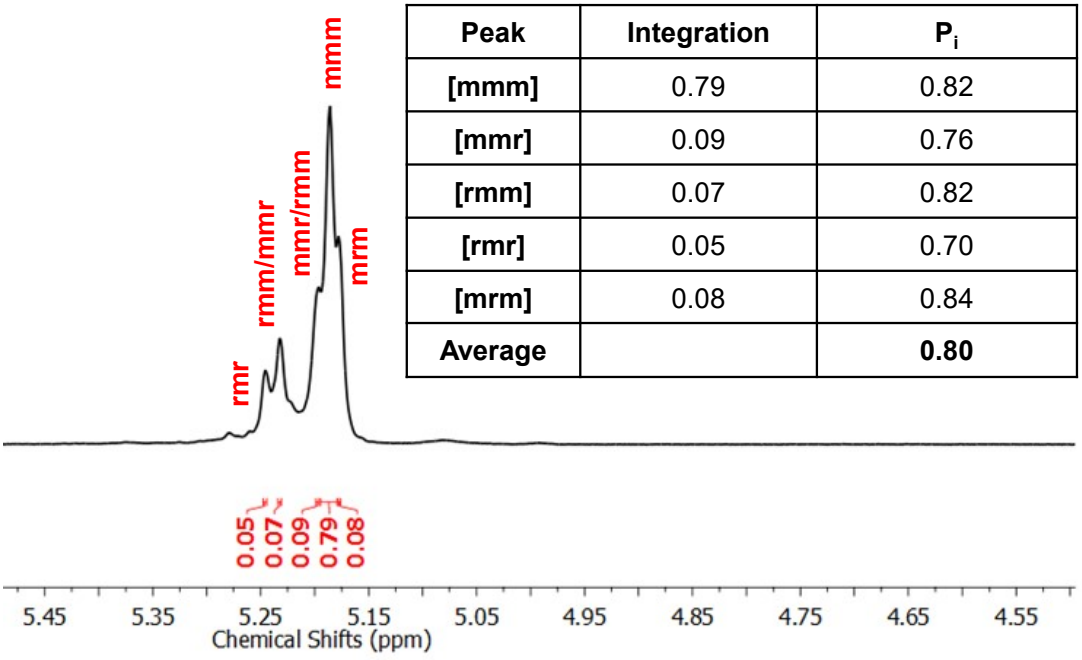

Peak	Integration	P_i
[mmm]	0.79	0.82
[mmr]	0.09	0.76
[rmm]	0.07	0.82
[rmr]	0.05	0.70
[mrm]	0.08	0.84
Average		**0.80**

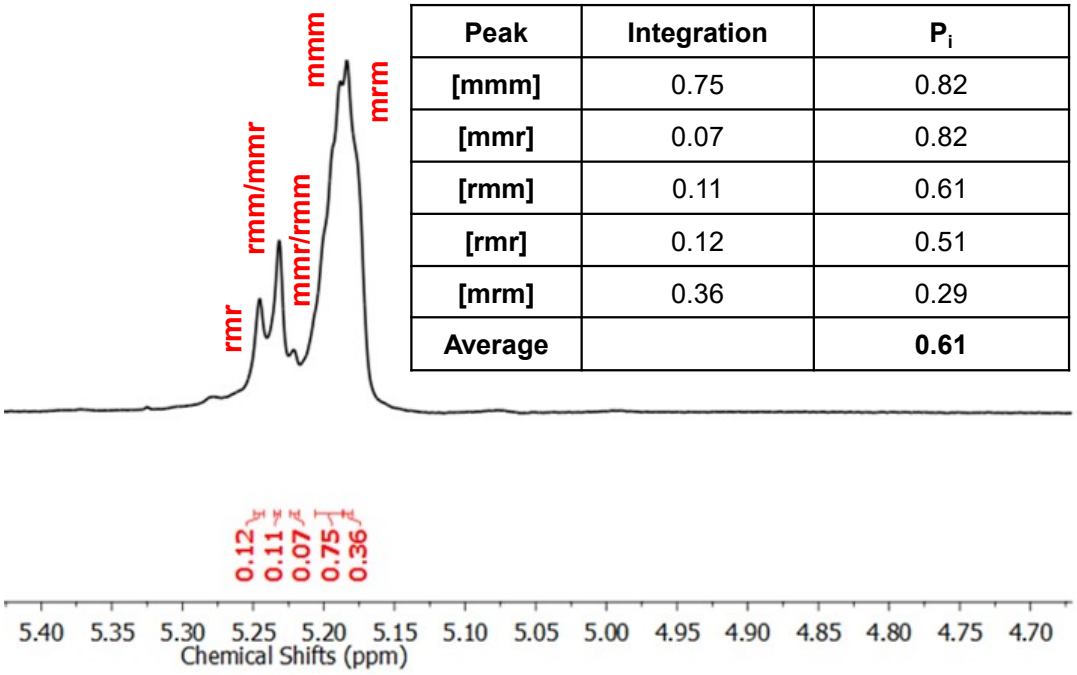

Peak	Integration	P_i
[mmm]	0.75	0.82
[mmr]	0.07	0.82
[rmm]	0.11	0.61
[rmr]	0.12	0.51
[mrm]	0.36	0.29
Average		**0.61**

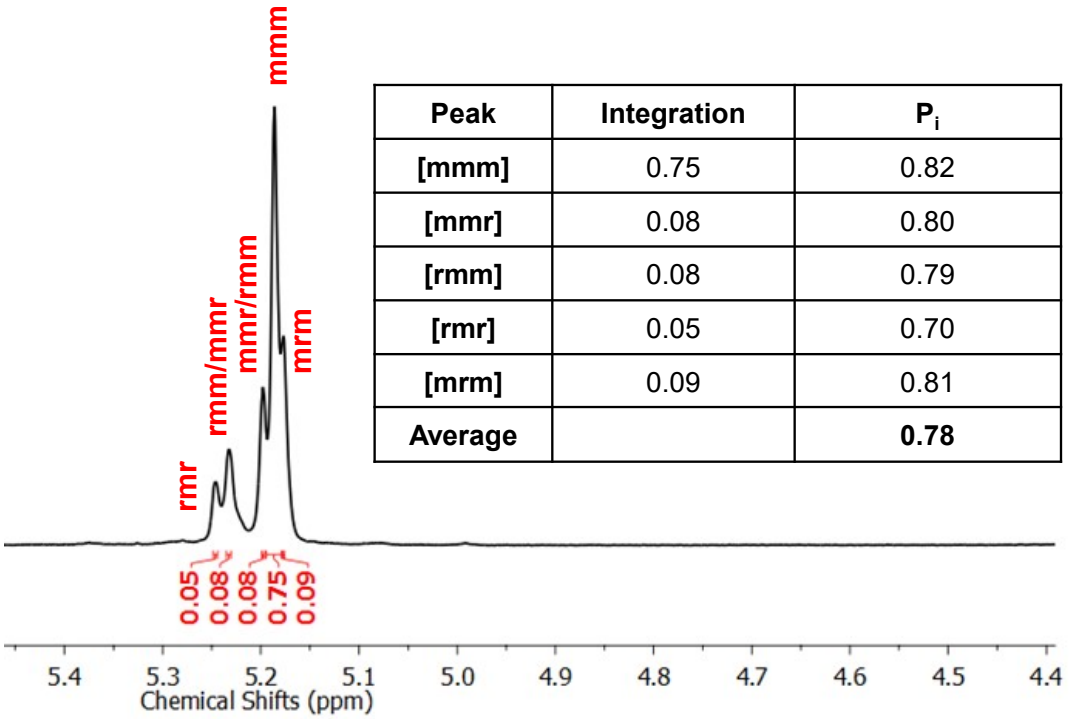

Peak	Integration	P_i
[mmm]	0.75	0.82
[mmr]	0.08	0.80
[rmm]	0.08	0.79
[rmr]	0.05	0.70
[mrm]	0.09	0.81
Average		**0.78**

Figure FS27. $^{1}H\{^{1}H\}$ NMR spectra ($CDCl_3$, 400 MHz, 25 °C) of methine regions for PLA [Entry 1, 2 and 4, Table TS11]

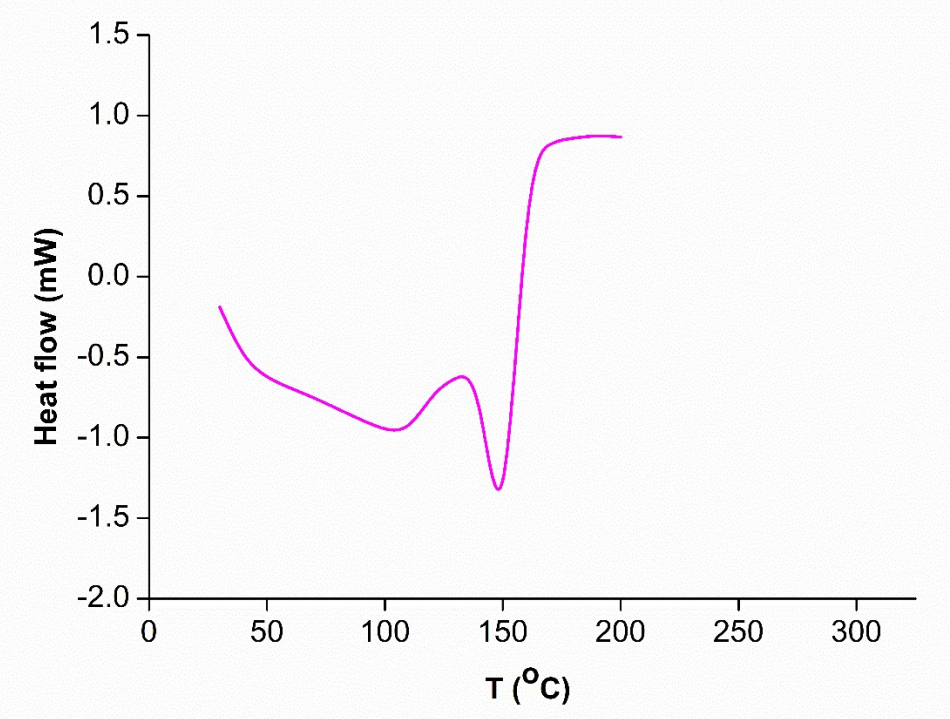

Figure FS28. DSC curve of PLA sample [Entry 4, Table TS11]

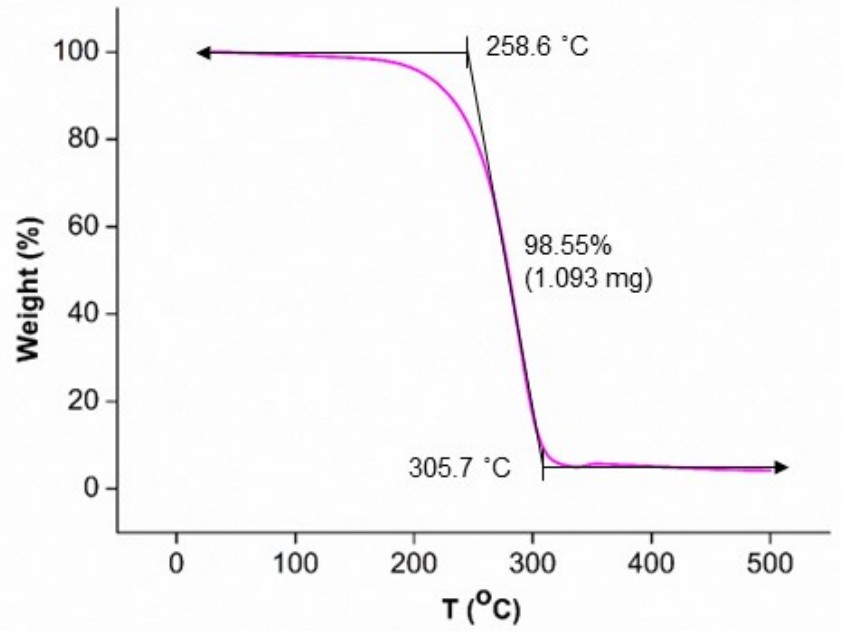

Figure FS29. TGA curve of PLA sample [Entry 4, Table TS11]

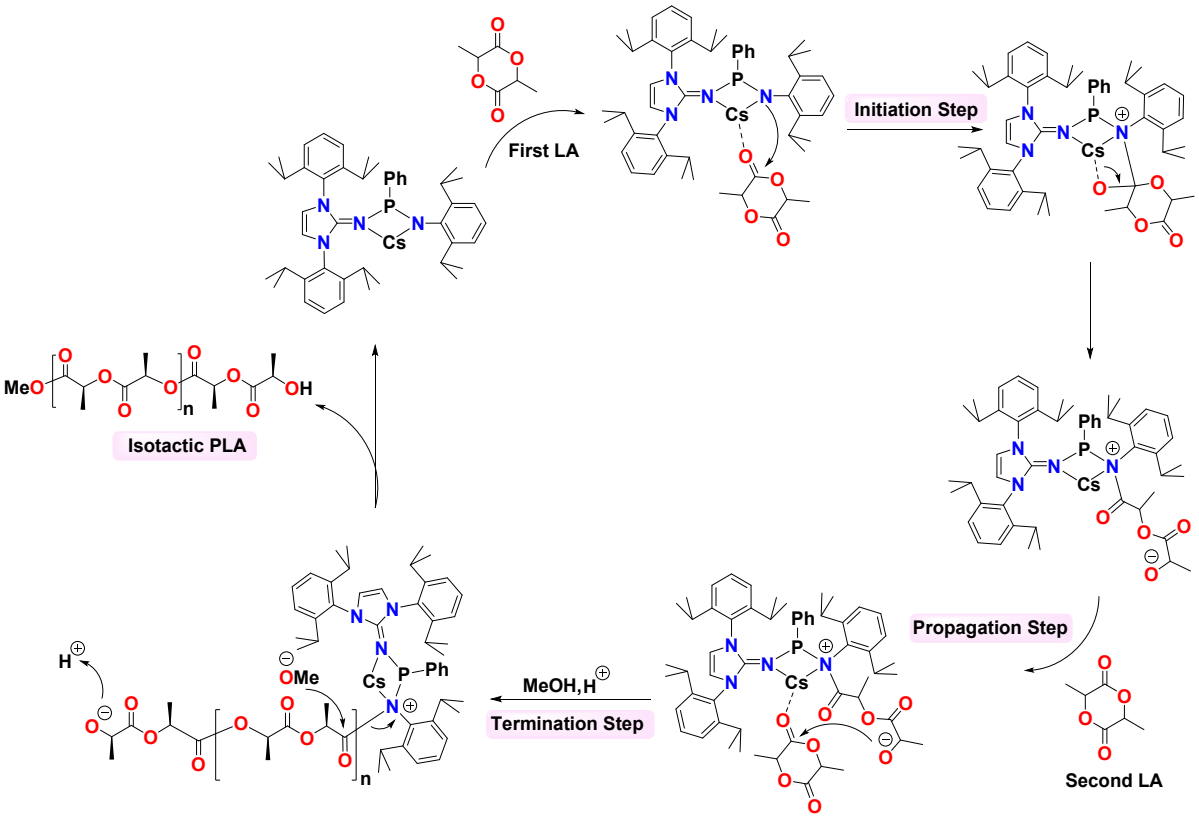

Figure FS30: ROP mechanism of *rac*-LA catalysed by catalyst **2**

Cha*rac*terisation of PCL

A typical polymerization procedure is exemplified by the synthesis of poly(ε-caprolactone) at ambient temperature (TableTS12). ε-CL (0.114 g, 0.8772 mmol) was added to a solution of **2** (0.007 g, 0.0087 mmol) in toluene (4 mL). After the desired reaction time, the monomer was converted into polymer, so the reaction was then quenched by the addition of a drop of 2 N HCl and methanol. Then solution was concentrated in vacuum and polymer was recrystallized with dichloromethane and hexane. The final polymer was filtered and dried under vacuum to constant weight.

Table TS14. ROP of ε-CL using catalyst **2**[a].

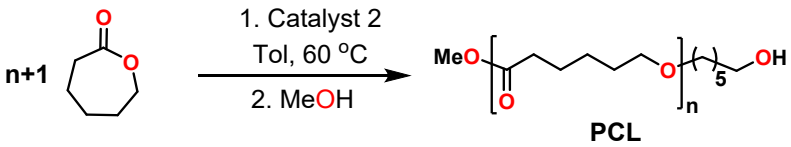

Entry	M:1	Time (h:m)	Conv[b]	Yield[c]	M_{ntheo} (kDa)[d]	M_{nexp}[e] (kDa)	PDI
1	100	00:30	97	99	11.2	11.6	1.1
2[f]	100	00:30	70	65	8.1	6.8	1.2
3[g]	100	00:30	95	96	10.9	6.9	1.6
4	200	00:30	96	99	22.0	22.8	1.1
5	300	00:30	96	97	32.9	36.3	1.3
6	400	00:30	97	96	44.4	52.1	1.1
7	500	00:30	95	96	54.2	55.7	1.3

[a]In toluene, [Catalyst] = 0.0087 mM, [b]Conversions were determined by ^{1}H NMR spectroscopy. [c]Isolated yield. [d]$M_{n\ (theo)}$= molecular weight of chain-end + 114 gmol-1 ×(M:1) × conversion. [e]In THF (2 mg mL^{-1}) and molecular weights were determined by GPC-LLS (flow rate ¼ 0.5 mL min^{-1}). [f]In THF as a solvent. Universal calibration was carried out with polystyrene standards, laser light scattering detector data, and concentration detector. Each experiment is duplicated to ensure precision. [g]In presence of initiator (BnOH).

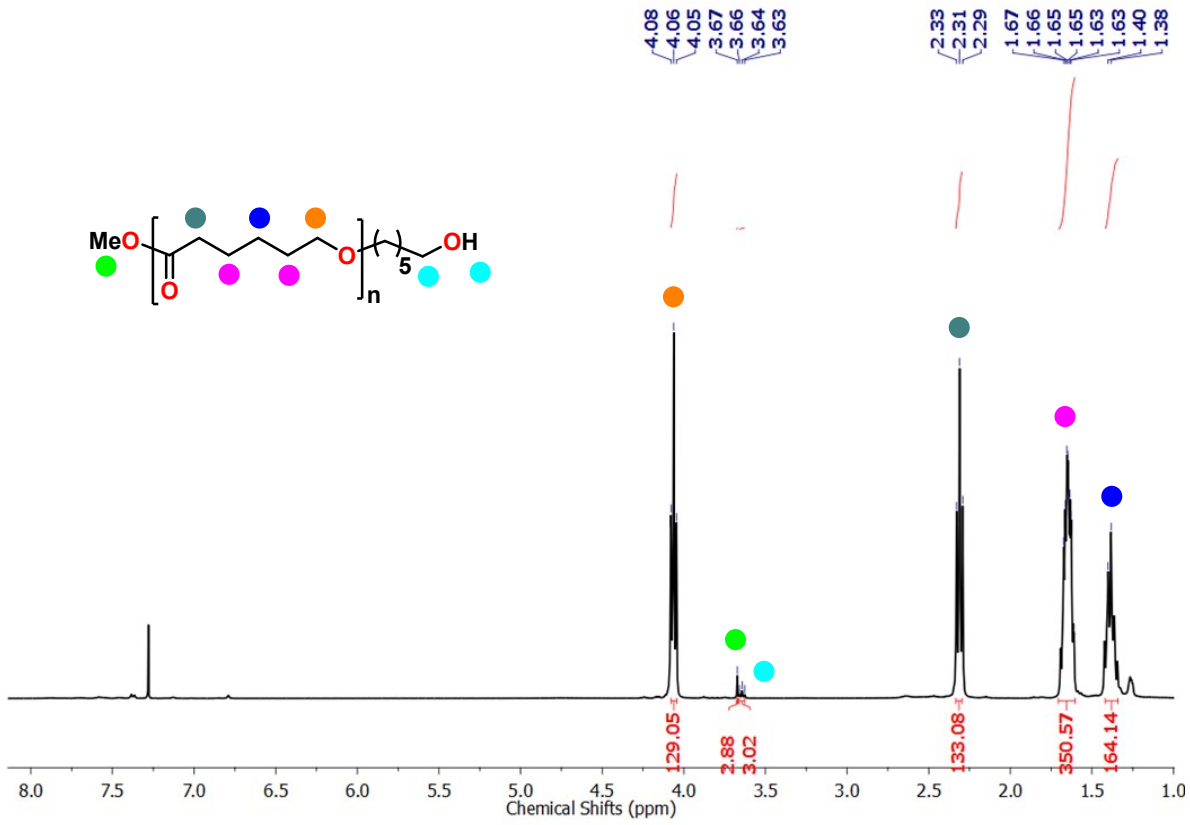

Figure FS31. ^{1}HNMR spectrum (400 MHz, 25°C, $CDCl_3$) of poly(ε-caprolactone) [Entry 1, Table TS14]

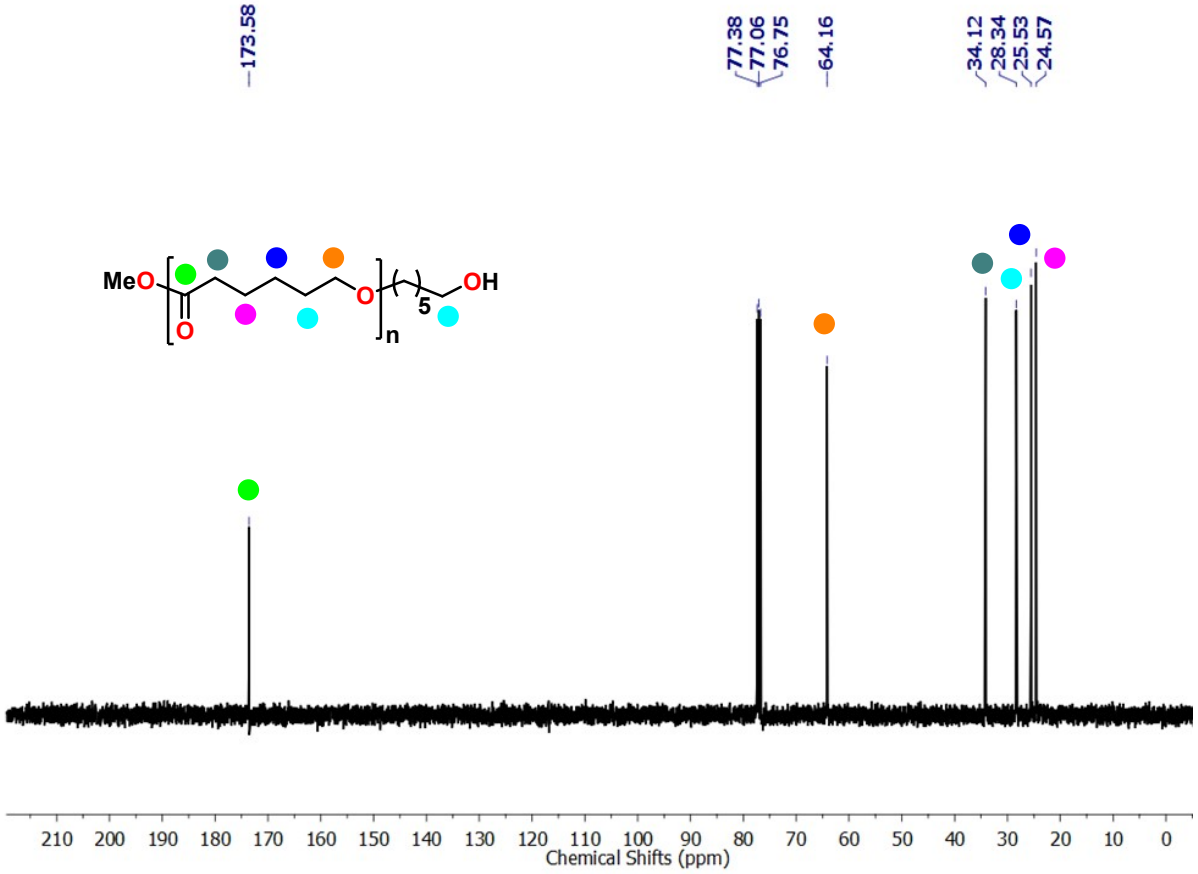

Figure FS32. ^{13}C NMR spectrum (100 MHz, 25°C, $CDCl_3$) of poly(ε-caprolactone) [Entry 1, Table TS14]

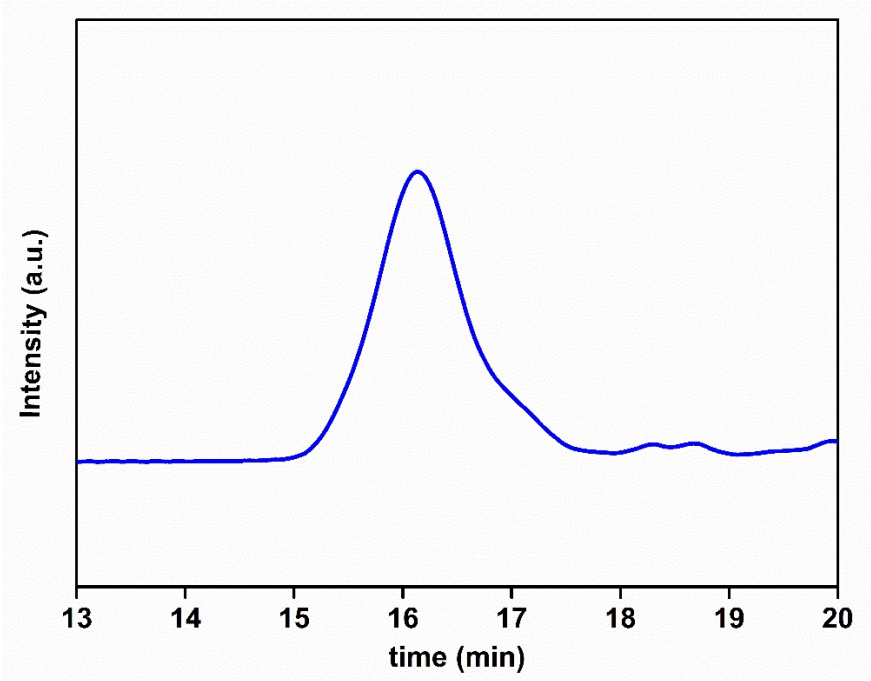

Figure FS33: GPC profile of PCL sample [Entry 1, Table TS14]

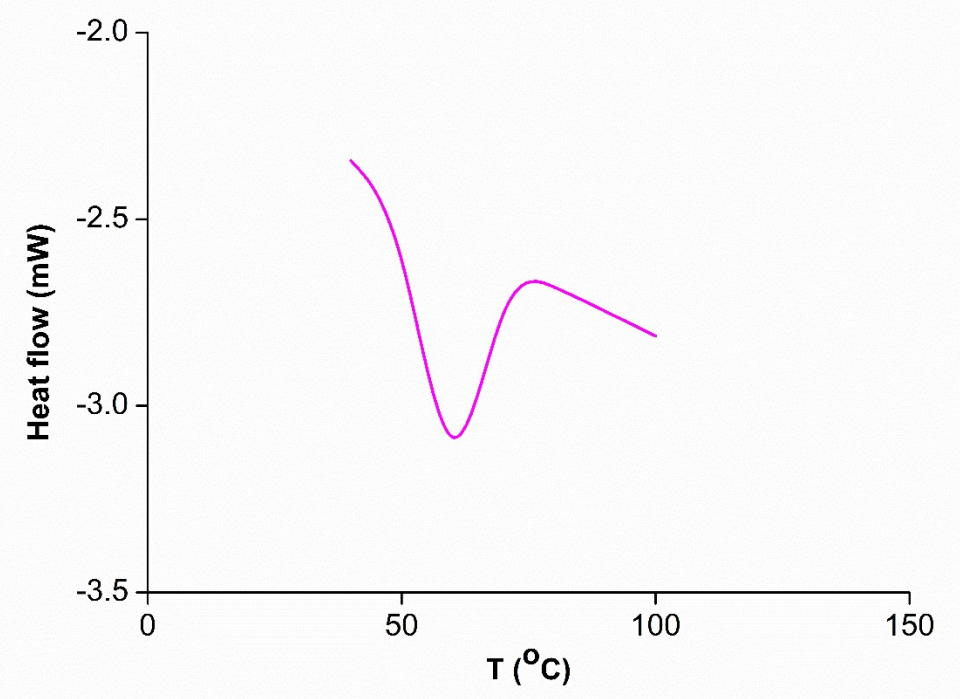

Figure FS34. DSC curves of PCL samples [Entry 4, Table TS14]

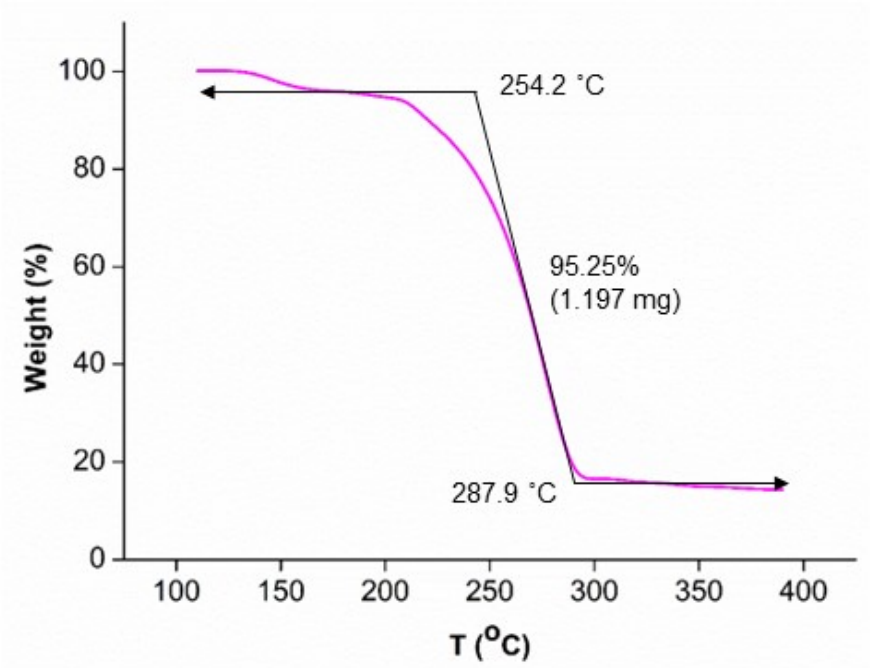

Figure FS35. TGA curves of PCL samples [Entry 4, Table TS14]

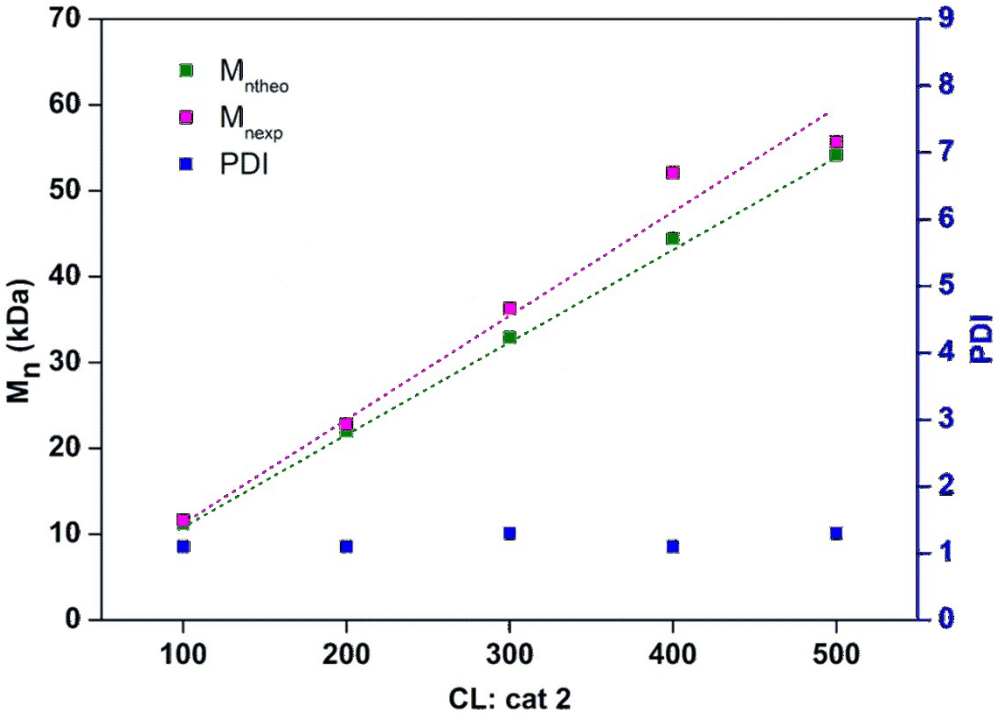

Figure FS36. Plot of theoretical, experimental M_n and molecular weight distribution of PCL as functions of added PCL with respect to catalyst **2** (M_n = number averaged molecular weight, PDI = polydispersity index). All reactions were carried out at room temperature in toluene, and conversion to polymer samples was >90%.

End group analysis:

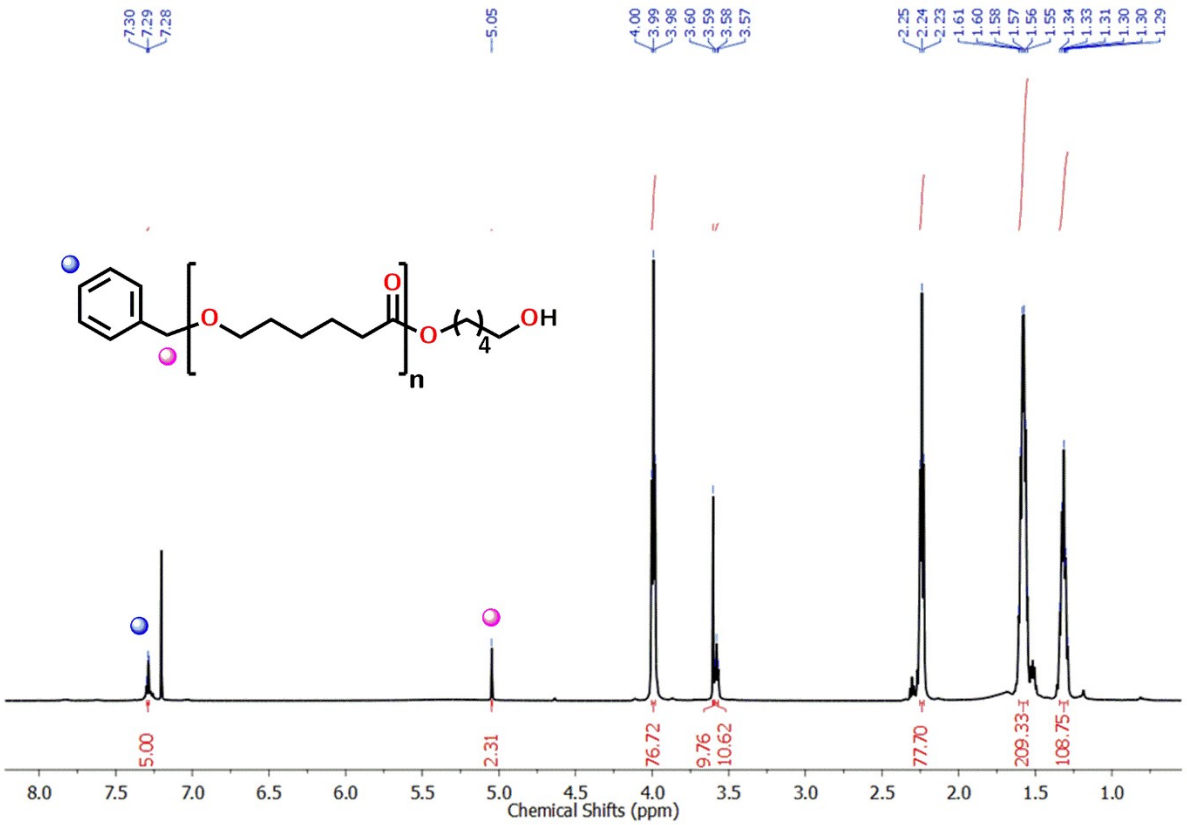

Figure FS37. ^{1}H-NMR spectra of PCL end capped by BnOH

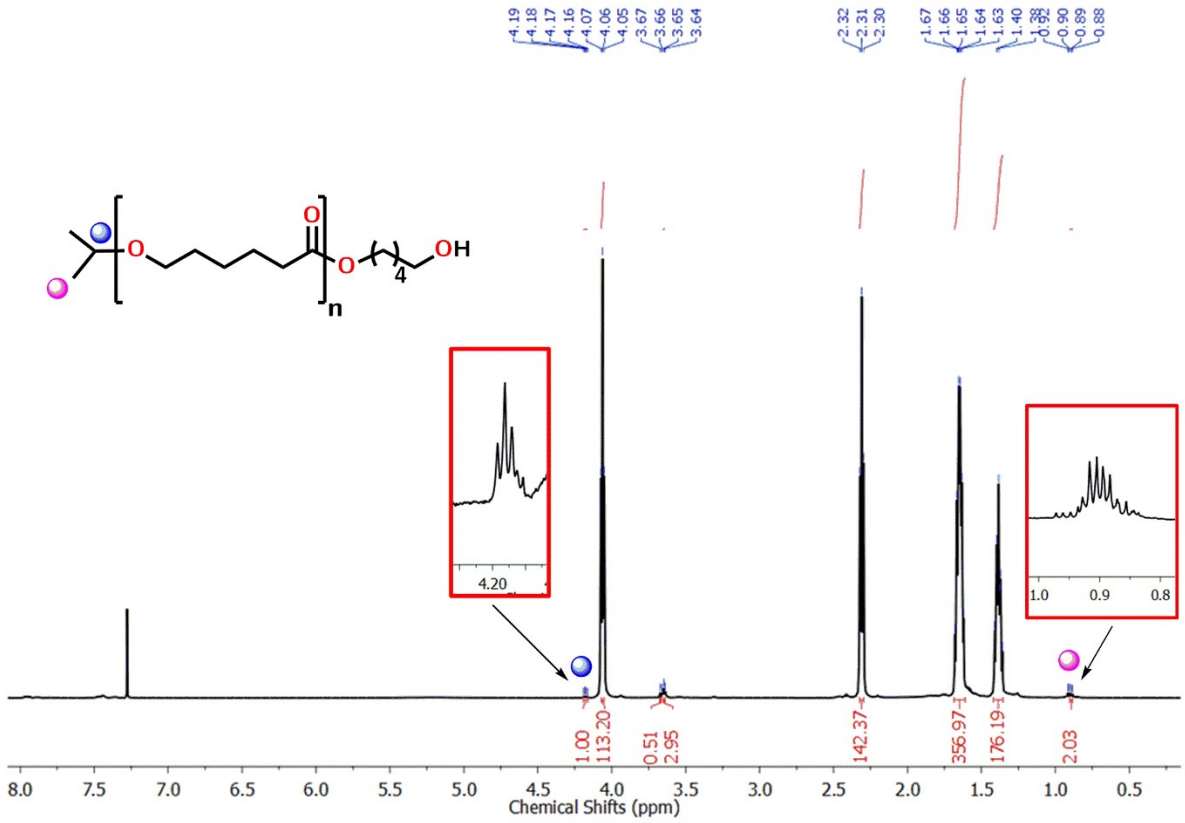

Figure FS38. ^{1}H-NMR spectra of PCL end capped by isopropyl alcohol.

Ring opening block copolymerization of *rac*-LA and ε-caprolactone

For a typical copolymerization procedure, *rac*-LA and ε-CL different [M:2] ratios, was added to a solution of cat **2** (0.008 g, 0.01 mmol) in toluene (4 mL). The solution was kept at stirring at 80 ˚C for different reaction time after which the reaction mixture was quenched by a drop of 2N HCl and methanol. Then after concentrating the solution under vacuum, the polymer was recrystallized from the mixture of dichloromethane and hexane. The final polymer was then dried under vacuum to constant weight.

Table TS15. Copolymerization of *rac*-LA and ε-CL using catalyst **2**[a]

Run	[CL]: [LA]:[2]	Time (h)	CL/LA[b] Conv (%)	CL/LA[c] (mol%)	Ratio of CL/LA: Terminal CL	M_{ntheo}[d] (kDa)	M_{nexp}[e] (kDa)	PDI	T_m (exp) ˚C
1	50:50:1	08	6/76	7/93	0.94	6.5	7.2	1.4	70.0
2	50:50:1	12	31/81	29/71	0.98	7.8	7.5	1.3	32.0
3	50:50:1	16	49/84	41/59	1.3	8.6	9.2	1.2	29.8
4	50:50:1	20	76/89	46/54	1.0	9.9	11.1	1.1	30.0
5	50:50:1	24	90/92	48/52	0.79	10.6	13.5	1.1	59.0
6[f]	50:50:1	24	24/85	21/79	0.92	7.9	8.4	1.9	28.3
7	40:60:1	24	88/96	39/61	1.0	10.3	10.4	1.1	60.0
8	75:25:1	24	86/98	71/29	0.83	12.3	12.8	1.4	60.4

[a]Reaction conditions: Tol (5 mL), 80 ˚C. [b]Percentage conversion of the monomer determined by ^{1}H NMR spectroscopy in $CDCl_3$. [c]CL/LA mole ratio in copolymer. [d]M_{ntheo} = ([CL]/[2] * %CL * 114.14*0.56) + ([LA]/[2] * % LA * 144.13*0.58). [e]Determined by GPC relative to polystyrene standards in tetrahydrofuran. Universal calibration was carried out with polystyrene standards, laser light scattering detector data, and concentration detector. Each experiment is duplicated to ensure precision.[f][CL]: [LA]:[**2**]:[BnOH] (50:50:1:1).

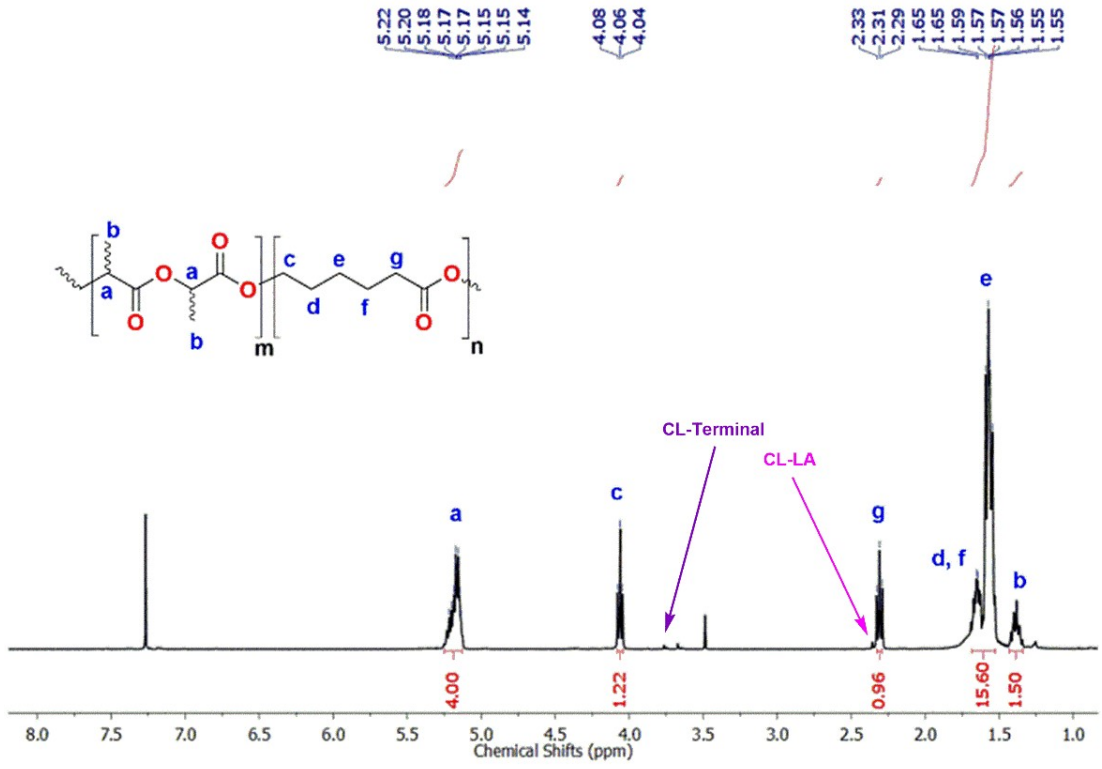

Figure FS39. ^{1}H NMR spectrum of a representative block copolymer (Run 4).

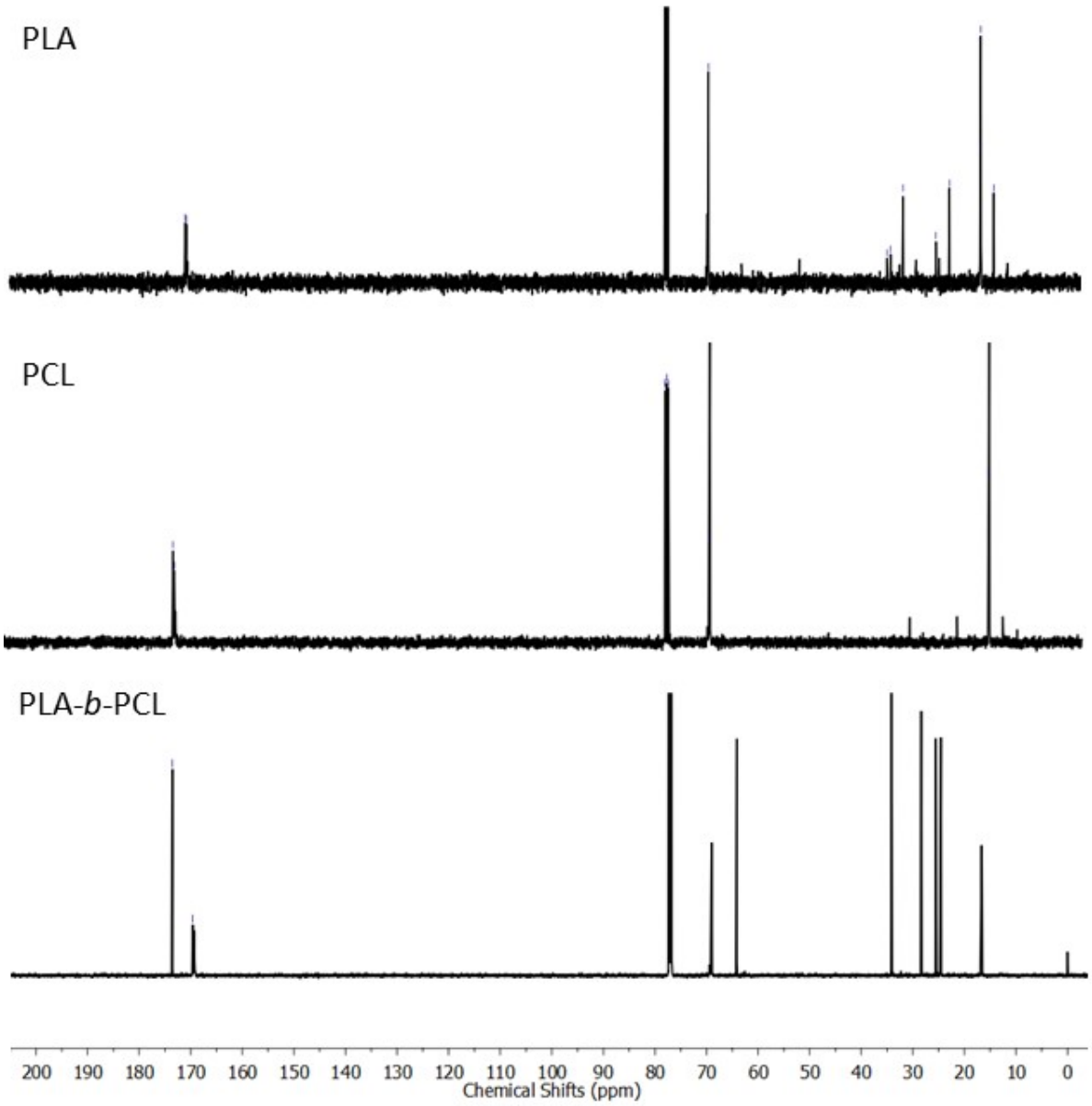

Figure FS40. ^{13}C NMR spectrum of a representative PLA, PCL and di-block copolymer (Run 4).

The spectra of ^{13}C-NMR (carbonyl region): It is observed that the products of reaction obtained show the chemical shift of the carbonyl groups in the same region of the homopolymers, that is, the presence of two signals corresponding to each carbonyl group of lactyl units (–O–CH–(CH_3)–C=O, d = 170 ppm) and caproyl units (–O–$(CH_2)_5$–C=O, d = 174 ppm), respectively. This indicates, without doubt, that the polymeric products obtained do not have random copolymer microstructures but rather that is a block copolymer (PLA-*b*-PCL).

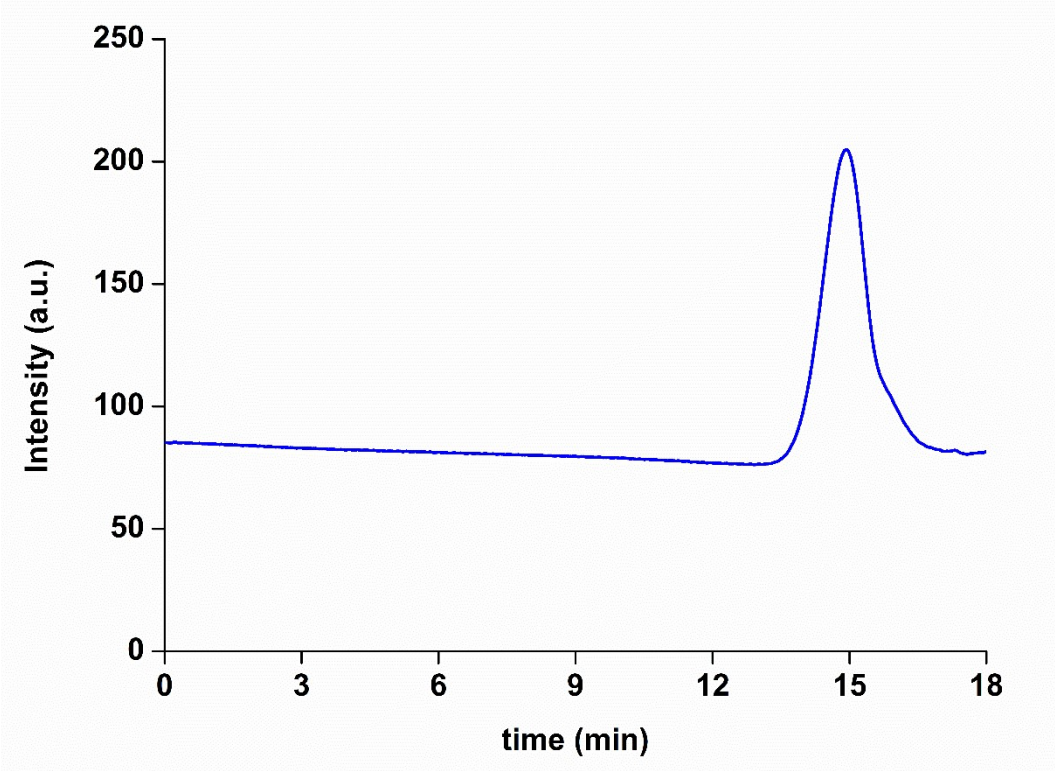

Figure FS41. GPC profile of copolymer samples [Entry 2, Table TS15]

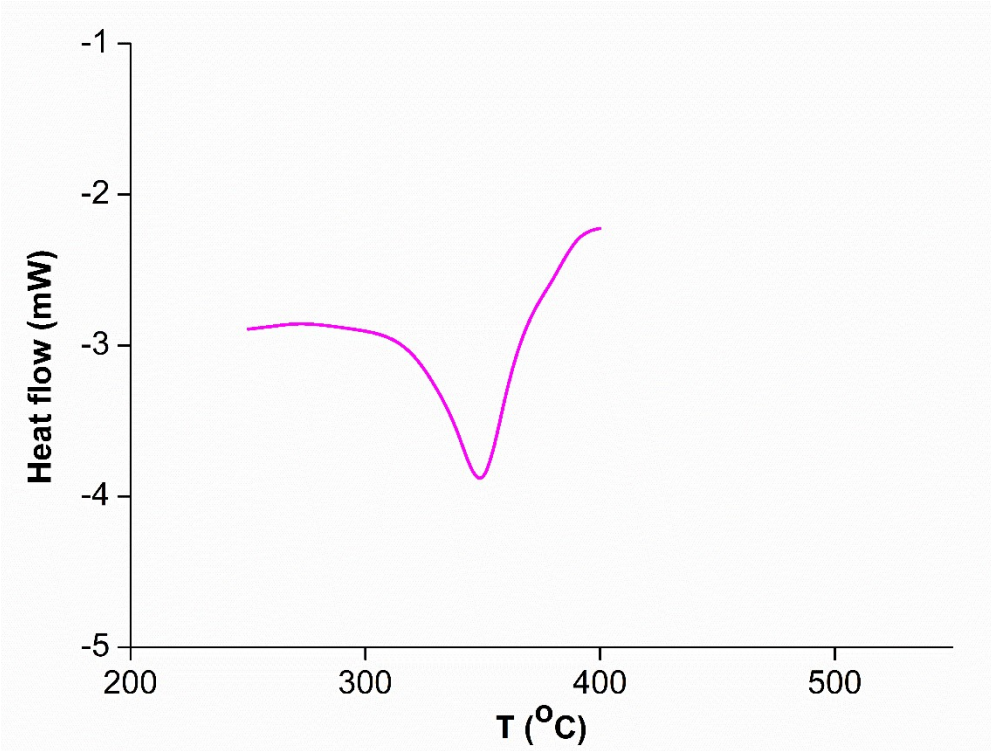

Figure FS42. DSC curve of a copolymer sample [Entry 2, Table TS15]

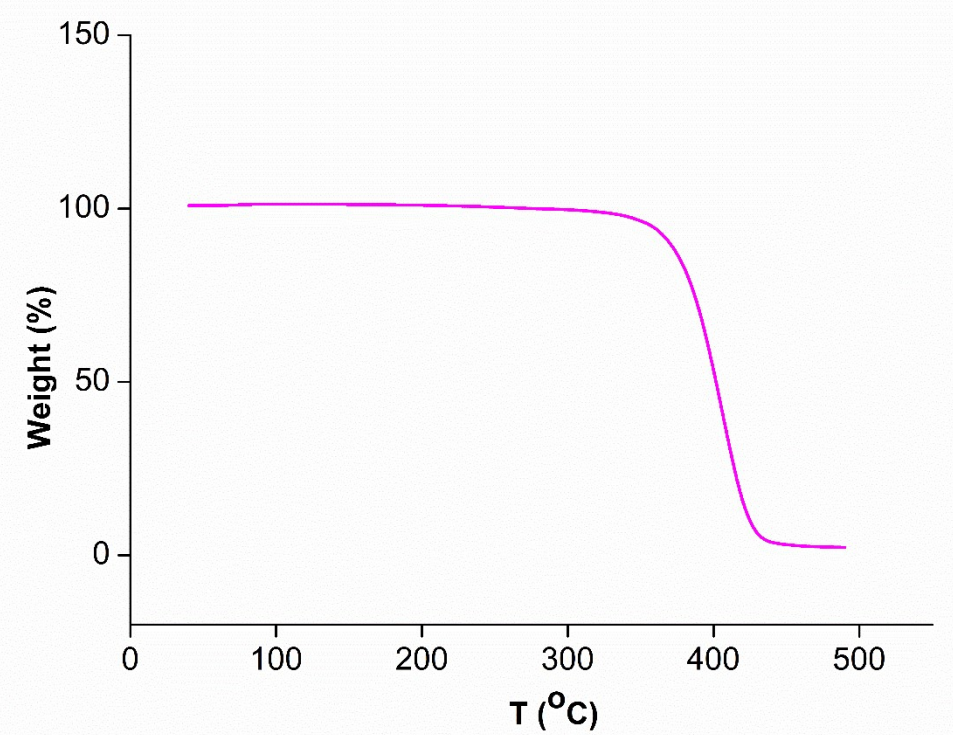

Figure FS43. TGA curve of a copolymer sample [Entry 2, Table TS15]

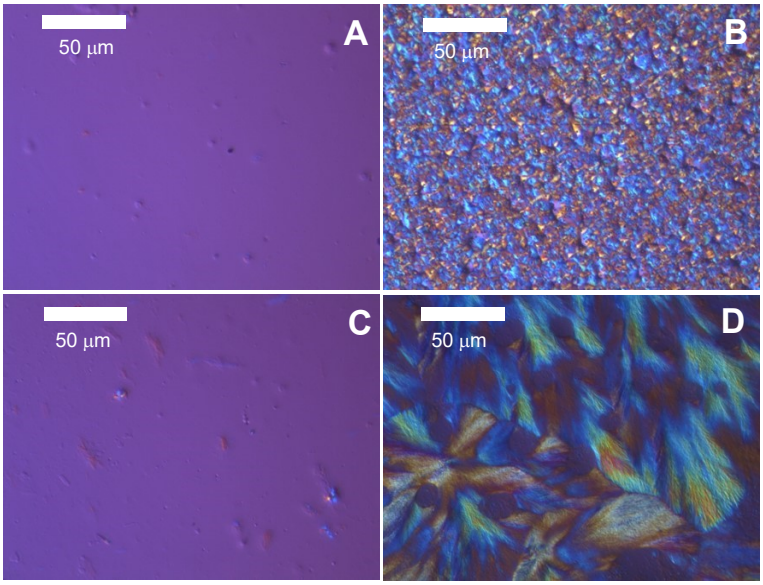

Figure FS44. Polarized Optical Micrographs of (A) pure PLA, (B) Pure PCL, (C) block copolymer with low PCL content (entry 1) and (D) block-copolymer with high PCL content (entry 3).

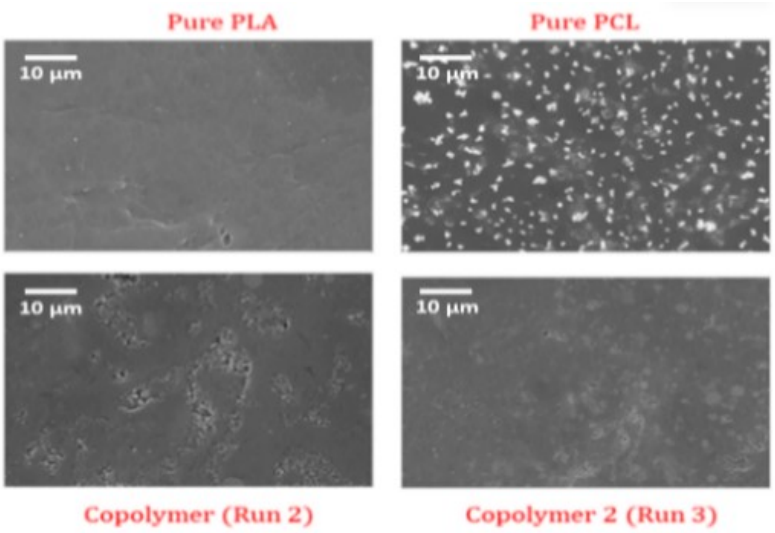

Figure FS45. Scanning electron microscopy (SEM) images of representative PLA, PCL and copolymers.

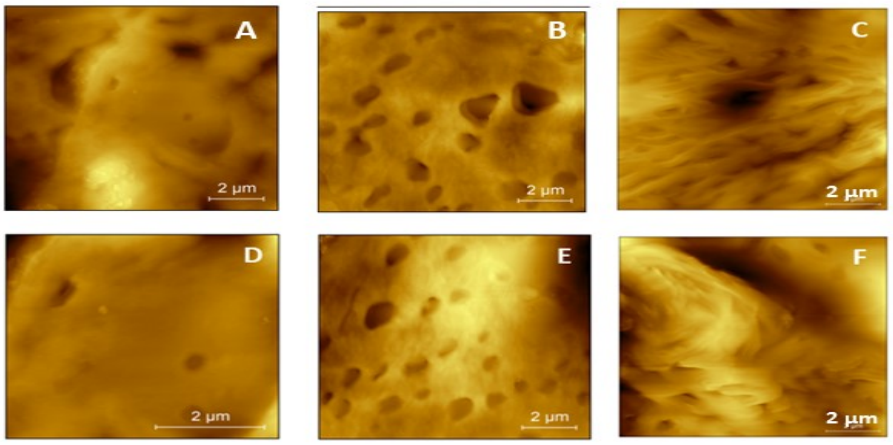

Figure FS46. Atomic Force Microscopy (AFM) images of representative PCL (A), PLA (B) and copolymers (C to F) runs 2 to 5.

References

1. S. Tabthong, T. Nanok, P. Kongsaeree, S. Prabpai and P. Hormnirun, *Dalton Transactions*, 2014, **43**, 1348–1359
2. J. Bhattacharjee, A. Sarkar and T. K. Panda, *Curr Opin Green Sustain Chem*, 2021, 31.
3. Arbaoui and C. Redshaw, *Polym Chem*, 2010, 1, 801–826.
4. Fang and H. Ma, *Eur Polym J*, 2019, **119**, 289–297.
5. H. Karmakar, S. Anga, T. K. Panda and V. Chandrasekhar, *RSC Adv*, 2022, **12**, 4501–4509.